JOURNAL OF NATURAL PRODUCTS

pubs.acs.org/jnp

Article

Transient Receptor Potential Melastatin 7 (TRPM7) Ion Channel Inhibitors: Preliminary SAR and Conformational Studies of Xenicane Diterpenoids from the Hawaiian Soft Coral *Sarcothelia edmondsoni*

Guangmin Yao, Matthew R. Parris, W. Cedric Kuo, Peter Pörzgen, Brandi Castillo, Evan S. Mason, Andres Chinchilla, Junhao Huang, Sayuri Suzuki, Rylee Ross, Ellis Akana, Savana Vander Schuit, Steven P. Miller, Reinhold Penner, Hong-Shuo Sun, Zhong-Ping Feng, Kenneth G. Hull, Daniel Romo,* Andrea Fleig,* and F. David Horgen*

Cite This: https://doi.org/10.1021/acs.jnatprod.3c00942

Read Online

ACCESS | Metrics & More | Article Recommendations | Supporting Information

ABSTRACT: Waixenicin A, a xenicane diterpene from the octocoral *Sarcothelia edmondsoni*, is a selective, potent inhibitor of the TRPM7 ion channel. To study the structure−activity relationship (SAR) of waixenicin A, we isolated and assayed related diterpenes from *S. edmondsoni*. In addition to known waixenicins A (**1**) and B (**2**), we purified six xenicane diterpenes, 7*S*,8*S*-epoxywaixenicins A (**3**) and B (**4**), 12-deacetylwaixenicin A (**5**), waixenicin E (**6**), waixenicin F (**7**), and 20-acetoxyxeniafaraunol B (**8**). We elucidated the structures of **3**−**8** by NMR and MS analyses. Compounds **1**, **2**, **3**, **4**, and **6** inhibited TRPM7 activity in a cell-based assay, while **5**, **7**, and **8** were inactive. A preliminary SAR emerged showing that alterations to the nine-membered ring of **1** did not reduce activity, while the 12-acetoxy group, in combination with the dihydropyran, appears to be necessary for TRPM7 inhibition. The bioactive compounds are proposed to be latent electrophiles by formation of a conjugated oxocarbenium ion intermediate. Whole-cell patch-clamp experiments demonstrated that waixenicin A inhibition is irreversible, consistent with a covalent inhibitor, and showed nanomolar potency for waixenicin B (**2**). Conformational analysis (DFT) of **1**, **3**, **7**, and **8** revealed insights into the conformation of waixenicin A and congeners and provided information regarding the stabilization of the proposed pharmacophore.

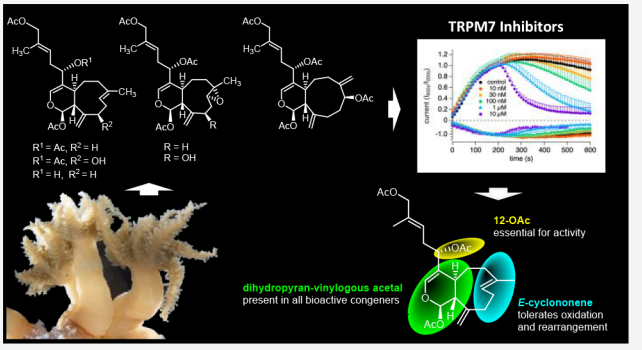

The soft coral *Sarcothelia edmondsoni* Verrill [family Xeniidae; order Alcyonacea; synonym: *Anthelia edmondsoni* (Verrill 1928)][1] is endemic to Hawai'i. Chemical studies on the genus *Sarcothelia* are rare. Two previous reports described the structure determination and/or the isolation of the xenicane diterpenoids waixenicins A−D[2,3] from *S. edmondsoni* (syn: *Anthelia edmondsoni*) but reported no biological activity. In the course of our search for ion channel inhibitors from chemical libraries derived from marine organisms,[4,5] the organic extract of *S. edmondsoni* was identified as a selective inhibitor of the seventh member of the melastatin-type transient receptor potential ion channel subfamily (TRPM7).[6]

TRPM7 is a ubiquitously expressed mammalian divalent cation channel that constitutes the principal mechanism for regulated Mg^{2+} entry into cells. Due to this critical function, TRPM7 is the only ion channel that is required for cell survival under normal growth conditions.[7] It is also unique in that the protein includes a functional kinase domain, which inhibits the channel conductance when bound to intracellular Mg^{2+} or Mg-ATP and thereby confers the ability to sense and respond to conditions of low intracellular Mg^{2+} and allow entry of divalent cations. The TRPM7 channel is abundantly expressed in a variety of human carcinomas,[8−12] and suppression of the channel by siRNA and/or inhibitors restrains cell growth. Moreover, high expression of TRPM7 was detected in breast cancer tissues, and the expression level correlates with the proliferative potential of breast cancer.[9] The involvement of TRPM7 in a variety of proliferative pathologies supports the investigation of TRPM7 as a potential therapeutic target for some cancers.

In another context, that of brain ischemia, TRPM7 abnormally conducts Ca^{2+} across the plasma membrane and plays a key role in Ca^{2+}-mediated neuronal death during

Received: October 6, 2023
Revised: March 2, 2024
Accepted: March 4, 2024

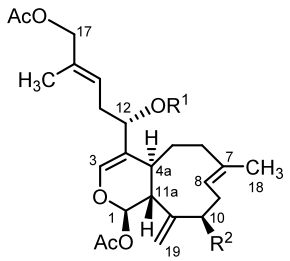

1: R^1 = Ac, R^2 = H
2: R^1 = Ac, R^2 = OH
5: R^1 = H, R^2 = H

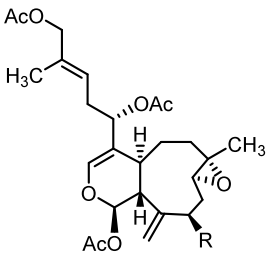

3: R = H
4: R = OH

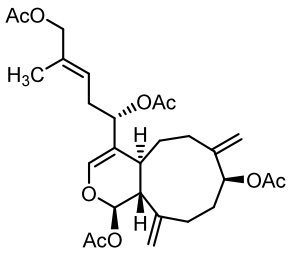

6

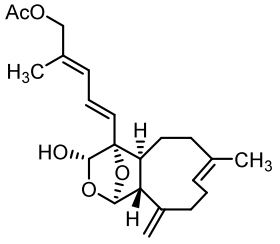

7

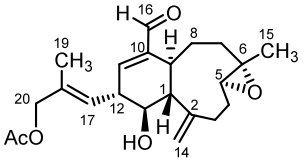

8

hypoxia/reperfusion injury. In fact, the expression of TRPM7 is upregulated after ischemia.[13] Anoxic neuronal death is attributed to elevated intracellular Ca^{2+} concentration after reperfusion[14] and is sustained due to a continuous influx of Ca^{2+} through TRPM7.[15] This conductance is independent of glutamate pathways, explaining the ineffectiveness of anti-excitotoxic therapies,[15] and is potentiated by low extracellular Ca^{2+}, low pH, and increased ROS/RNS production, which collectively are characteristic of an ischemic environment.[15,16] Most convincingly, silencing of TRPM7 with siRNA in both cell[15] and animal[16,17] ischemic models blocks the influx of Ca^{2+} and protects neurons from reperfusion injury. As such, TRPM7 is emerging as a promising target for ischemic disease.[17−20]

Despite the potential of TRPM7 as a target for intervention in cancer and ischemia/reperfusion injury, waixenicin A (**1**) remains the most potent and selective inhibitory modulator of the channel to date. Importantly, waixenicin A does not affect its highly homologous channel TRPM6.[6] Several nonspecific ion channel modulators can inhibit TRPM7 including lanthanum (La^{3+}),[21] 2-aminoethyl diphenylborinate,[22] spermine and other polyvalent cations,[24] gadolinium (Gd^{3+}),[25] carvacrol,[26] and 5-lipoxygenase inhibitors.[23] A viable and commercially available TRPM7 inhibitor is NS8593, which blocks channel activity with an IC_{50} of 1.6 μM in the absence of intracellular Mg^{2+}.[27] Under more physiological conditions of 780 μM free intracellular Mg^{2+}, we have recorded an IC_{50} for NS8593 of 3.9 μM (data not shown), which is aligned with previous findings at 300 μM free intracellular Mg^{2+} and an IC_{50} of 5.9 μM.[27] NS8593 is also a negative modulator of small conductance Ca^{2+}-activated K^+ ($K_{Ca}2$) channels[28] and, in addition, effectively inhibits TRPM7's sister channel TRPM6 at 10 μM.[29] Still, NS8593 has proven to be a valuable tool to probe for TRPM7 involvement in various disease models.[29−31] Similarly to NS8593, the cannabinoid cannabigerolic acid (CBGA) has been found to inhibit TRPM7 with an IC_{50} of 2.7 μM.[31] Systemic treatment of mice with CBGA ameliorates chronic kidney disease induced by ureteral obstruction and inhibits cisplatin-induced nephrotoxicity. This is likely due to CBGA's dual anti-inflammatory and anti-fibrotic activity paired with TRPM7 inhibition.[31,32] FTY720 is a clinically useful treatment for multiple sclerosis that, once phosphorylated, inhibits sphingosine 1-phosphate signaling,[33] but also inhibits TRPM7 in its nonphosphorylated form with an IC_{50} of 720 nM.[34] Recently, Chubanov and colleagues identified several compounds that are also able to differentiate between TRPM7 and its sister channel TRPM6.[29] The most promising compound, VER155008, is a purine nucleoside analog that inhibits heat shock protein 70[35] and inhibited TRPM7 with an IC_{50} of 110 nM in the absence of intracellular Mg^{2+} without affecting TRPM6. Unfortunately, Chubanov and colleagues only provide IC_{50} values under nonphysiological conditions in the absence of intracellular Mg^{2+}, so it remains unclear whether these compounds will be as effective in intact cells. These many TRPM7 inhibitors show promise, including as effective probes, but all exhibit reported bioactivities aside from TRPM7, prompting concerns about off-target effects.

Previously, we isolated waixenicin A (**1**) using bioassay-linked fractionation from an extract of *S. edmondsoni* that showed inhibitory activity in our TRPM7 marine natural products screening campaign. Waixenicin A (**1**) is currently the most potent (IC_{50} 16 nM) and the first reported selective inhibitor of TRPM7.[6] Extensive patch-clamp experiments showed that waixenicin A (**1**) potently blocks TRPM7 in a Mg^{2+}-dependent manner in both TRPM7-overexpressing and native cells. Cell cycle analysis indicated that waixenicin A (**1**) arrests cell growth in G0/G1, consistent with TRPM7 silencing. Furthermore, the inhibition is highly selective toward mammalian TRPM7 versus other TRP channels, including its closest homologue mammalian TRPM6[6] and zebra fish TRPM7,[36] for which waixenicin A (**1**) showed no effects on either channel's conductance in patch-clamp experiments at concentrations as high as 10 μM. Since the first report of its TRPM7 inhibitory activity, waixenicin A (**1**) has been used as a pharmacological tool for studying the role of TRPM7 in cancer,[11,37−40] malaria,[41] cystic and pulmonary fibrosis,[42,43] epilepsy,[44] and ischemic diseases.[17,18,45,46] Waixenicin A (**1**) has played a role in advancing TRPM7 as a potential drug target, especially for ischemic diseases, as it demonstrates exceptional selectivity and has good "drug likeness" with a molecular weight of 460 Da, no hydrogen-bond donors, 7 hydrogen bond acceptors, 10 rotatable bonds, and a calculated log*P* of 4.0.[47] Given its utility in inhibiting TRPM7 and drug-like physiochemical properties, the waixenicin A pharmacophore represents a potential lead compound for therapeutics based on TRPM7 inhibition, particularly toward novel intervention in cancer[48] and central nervous system (CNS) ischemic disease.[18] Recently, the interest in waixenicin A (**1**) as a starting point for drug development was punctuated by the first total synthesis, which established the absolute configuration of naturally occurring (+)-waixenicin A.[49]

In order to explore the structure−activity relationship (SAR) of the waixenicin A pharmacophore in inhibiting TRPM7 and to identify additional inhibitors, we conducted a systematic isolation of related diterpenes from an extract of *S. edmondsoni*.

https://doi.org/10.1021/acs.jnatprod.3c00942
J. Nat. Prod. XXXX, XXX, XXX−XXX

Here we report the isolation and structure determination of six xenicane diterpenoids (**3**−**8**), isolated together with the known compounds waixenicins A (**1**) and B (**2**). The comparative potency of compounds **1**−**8** in an established TRPM7 cell-based assay allowed us to construct a preliminary SAR for the inhibition of TRPM7 by waixenicin A. Conformational analysis of **1**, **3**, **7**, and **8** revealed a relatively constrained conformation of the bicyclic xenicin ring system that may define the waixenicin A pharmacophore's three-dimensional structure. The irreversible binding of waixenicin A was also established, and we propose generation of an oxocarbenium ion and capture by nucleophilic amino acid residues as a possible mechanism of covalent inhibition of TRPM7.

RESULTS AND DISCUSSION

Isolation and Structural Determination of Waixenicin A Analogs. The soft coral *S. edmondsoni* was collected off the east shore of Oahu, Hawaii, and immediately frozen. The soft coral biomass was freeze-dried and extracted with a CH_2Cl_2−methanol mixture to yield a dark green residue. The extract was subjected to MPLC over silica gel and then repeated reverse-phase HPLC to yield compounds **1**−**8**.

Compounds **1** and **2** were identified as (+)-waixenicins A (**1**) and B (**2**), respectively, by comparison of NMR (in benzene-d_6), MS data, and optical rotations with literature values.[3] The full ^{1}H and ^{13}C NMR assignments of both compounds in CD_3OD (Tables 1 and 2) were determined by ^{1}H, ^{13}C, ^{1}H−^{1}H COSY, and HSQC experiments.

Compound **3** has a molecular formula of $C_{26}H_{36}O_8$, as determined by HRESIMS and ^{13}C NMR, differing from **1** by one additional oxygen atom. Inspection of the ^{1}H and ^{13}C NMR spectra of **3** (Tables 1 and 2) revealed the absence of the Δ^7 double-bond signals, and in their place was the presence of signals consistent with an epoxide (δ_C 61.7, C-7; δ_C 64.2, C-8; δ_H 2.99, dd, H-8). The ^{1}H−^{1}H COSY correlations of H-8 and H_2-9 (δ_H 2.22, m; 1.51, m) and the HMBC correlations from H_3-18 (δ_H 1.33, s) to C-6 (δ_C 40.9), C-7, and C-8 confirmed the presence of an epoxide at C-7/C-8. The ROESY cross-peaks between H-8 and H-4a (δ_H 2.25 m), H-8 and H-6α, H_3-18 and H-11a (δ_H 2.45, m), H_3-18 and H-6β (δ_H 2.21, dt), H_3-18 and H-5β (δ_H 1.74, m), and H_3-18 and H-9β (δ_H 1.51, m) revealed that H_3-18 and H-8 were oriented *trans* on the nine-membered ring. Accordingly, the epoxide ring was assigned as 7*S**,8*S**. These along with further ROESY correlations, including H-11a to H-5β and H-4a to H-19$_{pro\text{-}Z}$ (δ_H 4.89, d), were consistent with the configuration and conformation of the crystal structure reported for the structurally similar waixenicin B (**2**),[1] which exposes the *si*−*si* face of the Δ^7 double bond to a position vulnerable to epoxidation that presumably leads to the 7*S*,8*S*-epoxide (see Figure 7 for the crystal structure of **2** and the calculated low-energy conformations for **1**). We assigned the relative orientation of the 12-OAc of **3** as α (*S*), consistent with the crystal structure of waixenicin B (**2**); we base this assignment on putative shared biosynthetic pathways and nearly identical NMR chemical shifts of **1**, **2**, and **3** for that section of the molecule (Tables 1 and 2).

Using identical arguments, compound **4** was identified as 7*S*,8*S*-epoxywaixenicin B. The molecular formula of $C_{26}H_{36}O_9$ was confirmed from HRESIMS and ^{13}C NMR data. The comparison of ^{1}H and ^{13}C NMR data of **2** and **4** (Tables 1 and 2) shows the same relationship as determined between **1** and **3**, indicating the absence of the *E*-double bond and the presence of an epoxide at C7/C-8 in **4**. This was confirmed by the ^{1}H−^{1}H COSY correlations between H-8 (δ_H 2.86, dd) and H_2-9 (δ_H 2.61, ddd; 1.46, ddd) and the HMBC correlations between H_3-18 (δ_H 1.41, s) and C-6 (δ_C 41.3), C-7 (δ_C 62.2), and C-8 (δ_C 62.5). The α-orientation of H-8 was deduced from the ROESY correlation between H-8 and H-4a (δ_H 2.12, m). Concurrently, the β-orientation of H_3-18 was deduced from the strong ROESY correlation between H_3-18 and H-11a (δ_H 2.80, br s). The *trans* configuration of H-8 and CH_3-18 requires an epoxide configuration of 7*S**,8*S**, as in compound **3**. In addition, the ROESY cross peaks from H-19$_{pro\text{-}E}$ (δ_H 4.94, s) to H-4a and H-5β (δ_H 1.89, m) to H-11a require a conformation of the nine-membered ring that is consistent with the crystal structure reported for waixenicin B (**2**)[1] and is discussed in detail below.

Compounds **3** and **4** are the corresponding epoxides of **1** and **2**, respectively. Coval and co-workers reported the 7,8-epoxide of waixenicin A as a product of pyridinium dichromate and air oxidations, without NMR or MS data. We also observed the partial conversion of waixenicin A (**1**) to 7,8-epoxywaixenicin A (**3**) after bubbling air through a methanolic solution for ∼24 h, and we regularly observed that storing waixenicins A (**1**) and B (**2**) as dry films at −20 °C leads to the slow conversion to their corresponding 7,8-epoxides as monitored by LC-MS (data not shown). Although the epoxidation of waixenicins A (**1**) and B (**2**) may well occur in *S. edmondsoni* or following natural release

Table 1. ^{1}H NMR Data (500 MHz, CD_3OD) for Waixenicins A (1) and B (2) and 7*S*,8*S*-Epoxywaixenicins A (3) and B (4)

	1	2	3	4
position	δ_H, multi, (*J* in Hz)	δ_H, multi, (*J* in Hz)	δ_H, multi, (*J* in Hz)	δ_H, multi, (*J* in Hz)
1	5.81, d (1.7)	5.83, d (2.1)	5.91, d (2.0)	5.97, d (1.2)
3	6.53, d (2.1)	6.51, d (3.2)	6.56, d (2.0)	6.55, d (2.0)
4a	2.17, m	2.13, br d (10.0)	2.25, br d (9.8)	2.12, m
5	2.03, m	2.05, m	α: 2.12, m	α: 2.13, m
	1.61, m	1.71, m	β: 1.74, m	β: 1.89, m
6	2.05, m	2.03, m	α: 1.14, m	α: 1.09, td (13.4, 4.3)
	2.22, m	2.24, m	β: 2.21, dt (13.3, 6.7)	β: 2.24, dt (13.3, 6.7)
8	5.38, m	5.18, m	2.99, dd (10.7, 3.9)	2.86, dd (2.2, 11.1)
9	2.51, m	2.49, m	α: 2.22, m	α: 2.61, ddd (14.5, 8.7, 4.1)
	2.09, m	2.44 m	β: 1.51, m	β: 1.46, ddd (14.7, 11.1, 1.5)
10	α: 2.31 m	4.42, d (7.3)	2.44, m	4.56, dd (8.5, 1.4)
	β: 2.29, m		2.40, m	
11a	2.01, s	2.49, br s	2.45, m	2.80, br s
12	5.34, t (7.6)	5.34, t (5.1)	5.33, t (7.4)	5.34, t (7.5)
13	2.52, m	2.52, m	2.53, m	2.51, m
	2.45, m	2.46, m	2.42, m	2.43, m
14	5.38, br t (7.1)	5.38, m	5.38, br t (7.1)	5.38, br t (6.6)
16	1.72, s	1.71, s	1.69, br s	1.68, s
17	4.44, s	4.44, s	4.44, s	4.44, s
18	1.69, s	1.78, s	1.33, s	1.41, s
19	4.78, d (1.5)	4.85, s	*pro-Z:* 4.89, d (0.9)	*pro-E:* 4.94, s
	4.89, br s	4.94, s	*pro-E:* 5.05, s	*pro-Z:* 5.12, s
1-OAc	2.01, s[a]	2.01, s[b]	2.06, s	2.05, s
12-OAc	2.02, s[a]	2.01, s[b]	2.01, s	2.01, s
17-OAc	2.04, s[a]	2.05, s[b]	2.05, s	2.04, s

[a,b]Signal may be interchanged.

https://doi.org/10.1021/acs.jnatprod.3c00942
J. Nat. Prod. XXXX, XXX, XXX−XXX

Table 2. ^{13}C NMR Data (125 MHz, CD_3OD) for Waixenicins A (1) and B (2) and 7*S*,8*S*-Epoxywaixenicins A (3) and B (4)

	1	2	3	4
position	δ_C	δ_C	δ_C	δ_C
1	92.8	93.4	92.4	93.1
3	141.8	142.0	142.4	142.7
4	116.8	117.0	116.8	117.0
4a	37.9	38.6	38.1	39.0
5	31.4	30.9	30.8	30.9
6	41.0	41.5	40.7	41.3
7	136.8	138.1	61.6	62.2
8	125.1	124.5	64.0	62.5
9	27.0	35.9	25.4	36.0
10	36.3	77.2	33.4	74.3
11	152.8	155.1	150.5	153.6
11a	50.4	42.9	48.6	41.9
12	75.6	76.0	75.4	75.9
13	31.6	31.8	31.8	32.0
14	124.4	122.5	124.5	124.7
15	134.1	134.2	134.5	134.6
16	14.6	14.5	14.4	14.6
17	70.4	70.5	70.5	70.7
18	17.0	17.5	16.8	17.2
19	113.5	113.4	115.1	114.9
1-OAc	170.8	170.8	171.1	170.9
	20.9	20.9	20.8	21.0
12-OAc	171.7[a]	172.0[b]	172.1	172.3
	21.0	21.4	21.3	21.4
17-OAc	172.1[a]	172.5[b]	172.5	172.8
	21.4	20.9	21.8	21.0

[a,b]Signals may be reversed.

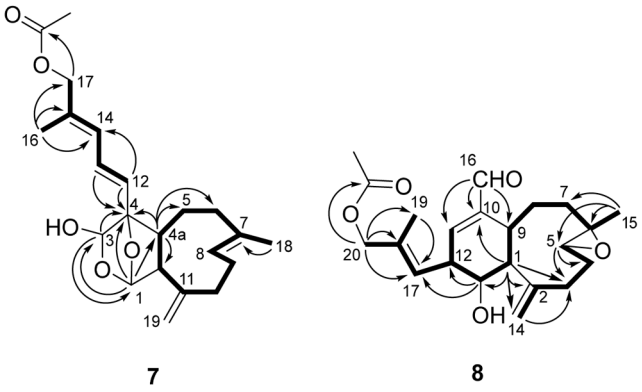

Figure 1. Key ^{1}H−^{1}H COSY (bold bonds) and HMBC correlations (→, H to C) for compounds **7** and **8**.

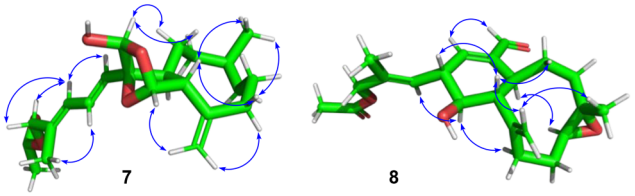

Figure 2. Observed NOE correlations (blue arrows) for waixenicin F (**7**) and 20-acetoxyxeniafaraunol B (**8**) from ROESY experiments depicted on the lowest energy conformers as determined through DFT calculations using a methanol continuum solvation model (B3LYP/6-31G, SMD-MeOH).

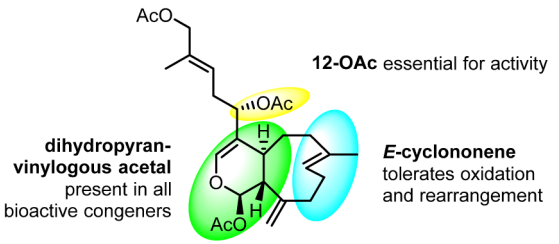

Figure 3. Preliminary structure−activity relationships for inhibition of TRPM7 by waixenicin A (**1**) analogs.

into the environment (following wounding for instance), the evidence suggests that at least some of our isolated waixenicin A and B epoxides (**3** and **4**, respectively) are artifacts of isolation. Nonetheless, these compounds add an important contribution to the structure−activity relationship of the waixenicin A pharmacophore as a TRPM7 inhibitor.

Compound **5** was identified as 12-deacetylwaixenicin A. Its molecular formula is $C_{24}H_{34}O_6$ as deduced from HRESIMS ([M + Na]$^+$, Δ −0.2 ppm) and NMR data. The ^{1}H and ^{13}C NMR spectra (Table 3) of **5** closely resemble those of waixenicin A (**1**), but **5** lacks one of the three acetyl groups found in **1**. The presence of a hydroxy in **5** in place of the 12-OAc in **1** was evident from ^{1}H and ^{13}C NMR chemical shifts of H-12 (δ_H 4.12, t) and C-12 (δ_C 74.0), respectively, in **5** that were less deshielded relative to those of waixenicin A (**1**). COSY, HSQC, and HMBC analyses confirmed that **5** is the 12-deacetyl analog of **1**, and the relative configuration of **5** was deduced to be identical to **1** based on similar optical rotation, ROESY correlations, and NMR chemical shifts (with the exception of those in close proximity to the 12-OAc) as well as the very likely shared biosynthetic origin.

Compound **6**, waixenicin E, was assigned a molecular formula of $C_{28}H_{38}O_9$ based on the HRESIMS of its sodium adduct (Δ +0.9 ppm). The ^{1}H and ^{13}C NMR spectra of compound **6** (Table 3) were similar to those of waixenicin A (**1**), with notable exceptions in the nine-membered ring. Namely, the olefinic methyl group on the nine-membered ring in **1** (C-18, δ_C 17.0) is replaced with a $\Delta^{7(18)}$-exocyclic double bond in **6** ($\delta_{C\text{-}7}$ 147.6; $\delta_{H\text{-}18}$ 5.30 and 5.19, $\delta_{C\text{-}18}$ 118.3), while the olefinic methine C-8 (δ_C 125.1; $\delta_{H\text{-}8}$ 5.38, m) of waixenicin A (**1**) is replaced by an acetoxy-substituted methine ($\delta_{C\text{-}8}$ 79.3; $\delta_{H\text{-}8}$ 5.26, dd) in waixenicin E (**6**). The positions of the exocyclic double bond and acetoxy-methine were determined by COSY and HMBC data. COSY peaks were observed between H-8 ($\delta_{H\text{-}8}$ 5.26) and H-9 (δ_H 2.01−2.03), while H-8 showed HMBC correlations to C-6 (δ_C 27.6), C-7 (δ_C 147.6), C-18 (δ_C 118.3), and the 8-OAc carbonyl (δ_C 171.9). In turn, H-18 protons (δ_H 5.19 and 5.30) showed HMBC correlations to C-8 and C-6. Together, these data firmly establish the gross structure of waixenicin E (**6**).

The relative configuration of **6** was established by analysis of ROESY correlations. An *E*-configuration was assigned to the Δ^{14} double bond based on the ROESY correlation between H-17 (δ_H 4.43) and H-14 (δ_H 5.30). ROESY correlations between H-4a (δ_H 2.45) and H-1 (δ_H 6.03) place H-4a and H-1 on the same face of the ring as in **1**. The correlation of both H-4a and H-1 to the *pro-Z* H-19 (δ_H 4.82) suggests a prominent conformation for **6** in which the H-11/H-19 exocyclic double bond is oriented similarly to that of **2** as established by the crystal structure of **2**.[3] Similarly, ROESY correlations between H-3 (δ_H 6.50) and both H-12 (δ_H 5.29) and H-13 (δ_H 2.53 and 2.37) are consistent with the α-orientation of 12-OAc. Finally, H-8 was assigned an α-

https://doi.org/10.1021/acs.jnatprod.3c00942
J. Nat. Prod. XXXX, XXX, XXX−XXX

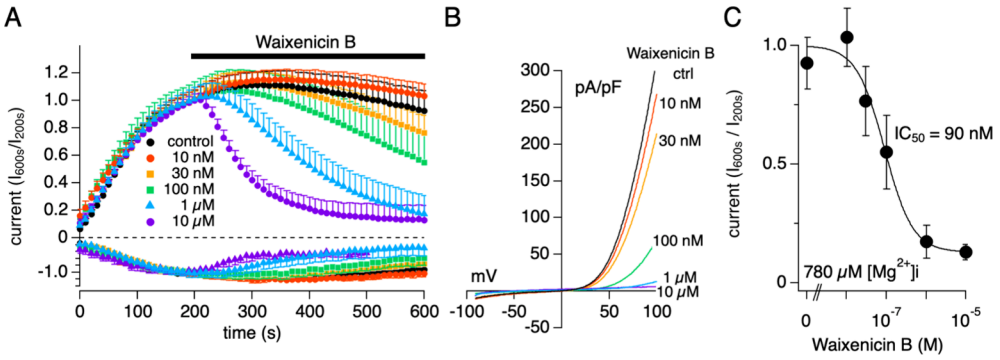

Figure 4. Waixenicin B (**2**) blocks TRPM7 currents in HEK293 cells induced to overexpress human TRPM7 (hTRPM7) in a dose-dependent manner. Error bars represent SEM. (A) Average inward (assessed at −80 mV) and outward hTRPM7 current densities (at +80 mV) in the presence of various concentrations of waixenicin B (n = 4−9). (B) Representative current/voltage (I/V) relationships for hTRPM7, under conditions described in A. All I/V relationships were analyzed at 600 s. (C) Dose−response curve for the inhibition of hTRPM7 currents by various concentrations of waixenicin B (**2**) (Hill coefficient = −1.2). Data points correspond to average current amplitudes measured at +80 mV at 600 s and normalized to 1 by dividing with current amplitudes at 200 s.

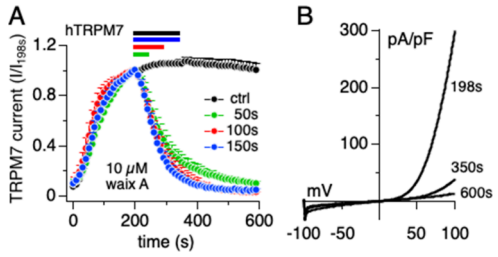

Figure 5. Time-dependent inhibition of hTRPM7 by waixenicin A (**1**). (A) Inhibitory effects of waixenicin A on TRPM7 currents were investigated by whole-cell patch-clamp recordings from HEK293 cells overexpressing human TRPM7 (hTRPM7). Average hTRPM7-mediated outward currents at +80 mV extracted from voltage ramp-evoked currents at 0.5 Hz and plotted as a function of time. Waixenicin A (10 μM) was applied at 200−250 s (green circles, n = 6), 200−300 s (red circles, n = 6), and 200−350 s (blue circles, n = 6). Each color bar indicates application time. Standard external Ringer (see Experimental Section) without waixenicin A-containing methanol as vehicle control (black circles, n = 7). (B) Average I/V curve of hTRPM7 currents extracted before (200 s) and after (350 s) 10 μM waixenicin A application and the end of recording (600 s) taken from an application time of 150 s (blue circles) in panel A.

orientation based on ROESY cross peaks with H-18, H-4a, and H-10α (δ_H 2.22). Accordingly, 8-OAc is assigned as β-oriented.

Compound **7**, waixenicin F, was isolated as a colorless oil. Its HRESIMS gave a sodium adduct (Δ +0.3 ppm) consistent with the molecular formula $C_{22}H_{30}O_5$, which requires eight degrees of unsaturation. The IR spectrum suggested the presence of hydroxy and carbonyl groups and carbon−carbon double bonds, while the UV spectrum suggested a conjugated diene system (λ_{max} 238 nm). The ^{1}H NMR spectrum (Table 4) revealed an *E,E*-diene system at $\delta_{H\text{-}12}$ 6.01 (d, J = 15.5 Hz), $\delta_{H\text{-}13}$ 6.76 (dd, J = 11.1, 15.5 Hz), and $\delta_{H\text{-}14}$ 6.16 (d, J = 11.1 Hz), an *exo*-methylene at $\delta_{H\text{-}19}$ 5.14 (s) and 4.82 (s), an olefinic proton at $\delta_{H\text{-}8}$ 5.29, two oxygenated methine protons at $\delta_{H\text{-}1}$ 5.21 (s) and $\delta_{H\text{-}3}$ 5.08 (s), one acetyl group methyl at δ_H 2.07 (s), and two methyl singlets at $\delta_{H\text{-}16}$ 1.83 and $\delta_{H\text{-}18}$ 1.69. The ^{13}C NMR and HSQC spectra confirmed the presence of an *E,E*-diene system, a trisubstituted double bond, an exocyclic double bond, one acetoxy group, two methyls, five methylenes (including one oxygenated methylene), four methines (including two oxygenated methines), and one oxygenated tertiary carbon. Four double bonds and one carbonyl account for five degrees of unsaturation, and the remaining three degrees of unsaturation indicate the presence of three rings in compound **7**.

Two partial structures (Figure 1) were established on the basis of the ^{1}H−^{1}H COSY and HSQC spectra of compound **7**. Connection of the *E,E*-diene system with the nine-membered ring through an oxygenated non-hydrogenated carbon C-4 was deduced by HMBC cross peaks from H-4a (δ_H 1.67), H-12, and H-13 to C-4 (δ_C 91.0) in **7**. The deshielding of signals for C-1 (δ_C 105.6) and C-3 (δ_C 94.5) and the HMBC correlation from H-1 to both C-3 and C-4a (δ_C 57.3), from both H-3 and H-11a (δ_H 1.79) to C-1, and from H-3 to C-4 suggested a six-membered ring connecting C-1/O/C-3/C-4/C-4a/C-11a in compound **7**, consistent with the xenicin carbon skeleton. The position of the exocyclic double bond on the nine-membered ring was confirmed by HMBC correlations from H-19α/β to C-10 (δ_C 37.4) and C-11a (δ_C 62.2). The acetoxyl group was placed at C-17 due to the cross peak from H-17 to the OAc carbonyl at δ_C 172.8 in the HMBC spectrum. Furthermore, the strong cross peak of H-1/C-4 in the HMBC spectrum indicated that C-1 (δ_C 105.6) was connected to the oxygenated carbon C-4 (δ_C 91.0) through an oxygen atom bridge, which meets the requirement of the eight degrees of unsaturation and explains the low chemical shifts of C-1 and C-4.

The relative configuration of compound **7** was determined by analysis of its ROESY, as shown in Figure 2 and Table 4. The *E,E*-diene was confirmed by the ROESY correlations between H-14 and both H-12 and H-17 and between H-13 and H-16. The *E* configuration of Δ^7 was deduced from ROESY correlations between H-18 with H-9β and between H-8 and H-6α. The strong ROESY correlations of H-3 with H_2-5 revealed that H-3 and C-5 are on the same face of the ring and H-3 is β-oriented, while the 3-OH and H-4a are α-oriented. ROESY correlations from H-4a to both H-8 and H-19α and from methyl H-18 to H-11a indicated that H-11a was in the β orientation. The presence of a ROESY correlation between H-1 and H-11a suggests that H-1 and H-11a are *cis* to each other on the six-membered ring and are in the β orientation.

Together, the data indicate compound **7** is a novel xenicin diterpenoid with an oxygen atom bridge between C-1 and C-4 in the six-membered tetrahydropyran ring, and compound **7** was named waixenicin F.

Compound **8** was isolated as a colorless oil. In the (−)-ESIMS, it gave adduct peaks at m/z 409/411 $[M + Cl]^-$

https://doi.org/10.1021/acs.jnatprod.3c00942
J. Nat. Prod. XXXX, XXX, XXX−XXX

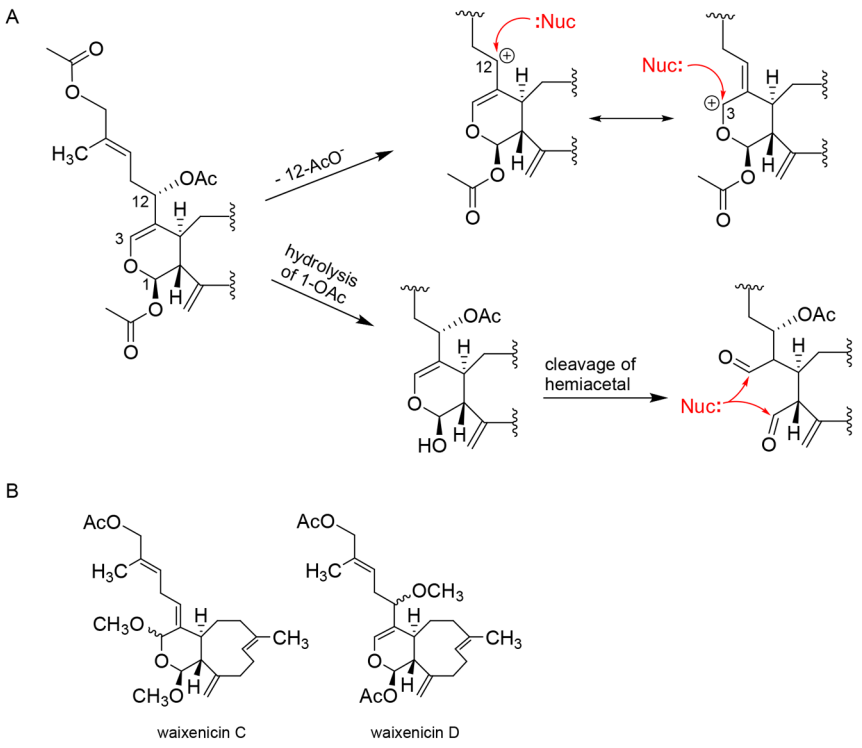

Figure 6. (A) Proposed electrophilicity and covalent binding mechanisms for the waixenicin A pharmacophore. Loss of the C-12 acetoxy results in a resonance-stabilized oxocarbenium cation that is electrophilic at C-3 and C-12. Hydrolysis of the C-1 acetate gives a hemiacetal that opens to an aldehyde and enol, the latter of which would readily tautomerize into a 1,5-dialdehyde. (B) Structures of waixenicins C and D.

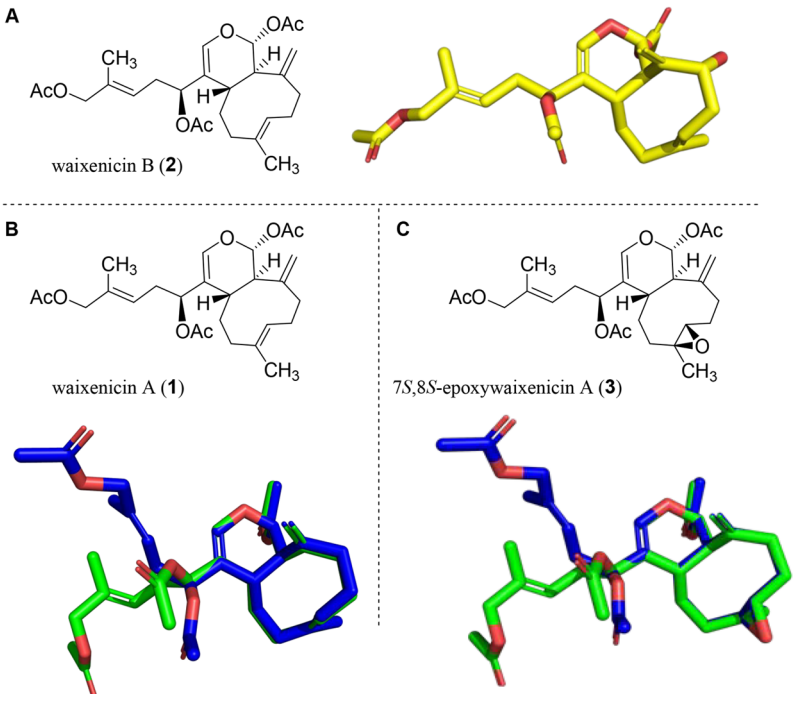

Figure 7. (A) Chemical structure and single-crystal X-ray structure of waixenicin B (**2**).[3] (B) Chemical structure of waixenicin A (**1**) and overlay of two low-energy conformers identified through MOE followed by DFT calculations. (C) Chemical structure of 7*S*,8*S*-epoxywaixenicin A (**3**) and overlay of two low-energy conformers identified through MOE followed by DFT. All DFT calculations were performed using a methanol continuum solvation model (B3LYP/6-31G, SMD-MeOH).

and 419 $[M + HCOO]^-$, indicating a molecular weight of 374. The molecular formula of $C_{22}H_{30}O_5$, requiring eight degrees of unsaturation, was deduced from HRESIMS in positive mode ($[M + Na]^+$, Δ +1.0 ppm) in conjunction with ^1H NMR and ^{13}C NMR data (Table 5). The IR spectrum of **8** suggested the presence of a hydroxy (ν_{max} 3445 cm^{-1}), an ester carbonyl (ν_{max}

https://doi.org/10.1021/acs.jnatprod.3c00942
J. Nat. Prod. XXXX, XXX, XXX−XXX

Table 3. ^{1}H and ^{13}C NMR Data (500/125 MHz, CD_3OD) for 12-Deacetylwaixenicin A (5) and Waixenicin E (6)

	5		6	
position	δ_C, type	δ_H (J in Hz)	δ_C, type	δ_H (J in Hz)
1	93.6, CH	5.79, d (2.0)	94.5, CH	6.03, d (4.5)
3	139.8, CH	6.39, d (2.0)	142.9, CH	6.50, d (1.4)
4	120.7, C		115.5, C	
4a	38.1, CH	2.21, m	34.3, CH	2.45, m
5	32.1, CH_2	α: 2.24, m	31.3, CH_2	α: 2.21, m
		β: 1.55, m		β: 1.85, m
6	41.2, CH_2	α: 2.09, m	27.6, CH_2	α: 2.23, m
		β: 2.18, m		β: 2.42, m
7	137.3, C		147.6, C	
8	125.2, CH	5.39, t (8.1)	79.3, CH	5.26, dd (6.2, 8.6)
9	26.2, CH_2	α: 2.09, m	30.3, CH_2	2.01, m
		β: 2.51, m		2.03, m
10	36.5, CH_2	α: 2.29, m	32.7, CH_2	α: 2.22, m
		β: 2.29, m		β: 2.34, m
11	153.4, C		149.1, C	
11a	51.2, CH	2.01, br s	41.7, CH	2.88, t (4.5)
12	74.0, CH	4.12, t (7.5)	75.6, CH	5.29, t (7.5)
13	34.2, CH_2	2.41, m	31.8, CH_2	2.53, m
		2.41, m		2.37, m
14	126.4, CH	5.41, t (6.2)	124.7, CH	5.30, m
15	133.2, C		134.5, C	
16	14.6, CH_3	1.71, s	14.6, CH_3	1.70, s
17	71.1, CH_2	4.44, s	70.7, CH_2	4.43, s
18	17.1, CH_3	1.68, s	118.3, CH_2	*pro-Z:* 5.19, s
				pro-E: 5.30, s
19	113.7, CH_2	*pro-Z:* 4.85, s	112.8, CH_2	*pro-Z:* 4.82, s
		pro-E: 4.80, d (1.4)		*pro-E:* 4.95, s
1-OAc	171.6, C		171.1, C	
	21.0, CH_3	2.05, s	21.0, CH_3	2.04, s
8-OAc			171.9, C	
			21.3, CH_3	2.01, s
12-OAc			172.3, C	
			21.5, CH_3	2.02, s
17-OAc	172.8, C		172.7, C	
	21.1, CH_3	2.03, s	21.0, CH_3	2.05, s

1734 cm^{-1}), a conjugated carbonyl (ν_{max} 1678 cm^{-1}), and carbon−carbon double bonds (ν_{max} 1632 cm^{-1}). The strong UV absorption at 233 nm further supported the existence of a conjugated system in the molecule.

The ^{1}H NMR spectrum of compound **8** showed the presence of one tertiary methyl group ($\delta_{H\text{-}15}$ 1.23, s), one vinyl methyl group ($\delta_{H\text{-}19}$ 1.79, d), one acetyl methyl group (δ_H 2.06, s), one disubstituted exocyclic double bond ($\delta_{H\text{-}14}$ 5.11, s; 5.16, s), one trisubstituted double bond ($\delta_{H\text{-}17}$ 5.39, dd), and one α,β-unsaturated aldehyde ($\delta_{H\text{-}11}$ 6.41, br s; $\delta_{H\text{-}16}$ 9.36, s). The ^{13}C NMR spectrum indicated an epoxide ($\delta_{C\text{-}5}$ 65.7; $\delta_{C\text{-}6}$ 62.1), a trisubstituted double bond ($\delta_{C\text{-}17}$ 129.5; $\delta_{C\text{-}18}$ 135.6), an exocyclic double bond ($\delta_{C\text{-}2}$ 148.2; $\delta_{C\text{-}14}$ 119.6), one α,β-unsaturated aldehyde ($\delta_{C\text{-}10}$ 147.9; $\delta_{C\text{-}11}$ 152.0; $\delta_{C\text{-}16}$ 195.8), one acetyl carbonyl (δ_C 172.8), one acetyl methyl (δ_C 20.9), two other methyls ($\delta_{C\text{-}19}$ 14.9; $\delta_{C\text{-}15}$ 19.5), five methylenes (including one oxygenated methylene), and four methines (including one oxygenated methine). The aldehyde carbon, acetyl carbonyl, and three double bonds accounted for five degrees of unsaturation; the remaining three degrees of unsaturation in **8** were consistent with a tricyclic diterpenoid (including the epoxide).

$^{1}H-^{1}H$ COSY (including a 'W'-type correlation) and HSQC allowed us to distinguish two spin systems in **8** (Figure 1), including one conjugated aldehyde and one acetyl group. An HMBC experiment was used to assemble the partial structures through fully substituted carbons and heteroatoms. The connection of C-1 with C-2 was deduced from HMBC correlations between H-1 (δ_H 2.26, t) and C-3 (δ_C 27.7), C-2, and C-14 and correlations between exocyclic double-bond protons H-14 and both C-1 (δ_C 61.4) and C-3. Cross peaks between H-15 (δ_H 1.23, s) and C-7 (δ_C 39.9) and epoxide carbons ($\delta_{C\text{-}5}$ 65.7, $\delta_{C\text{-}6}$ 62.1), as well as correlations between H-7 (δ_H 1.57, dd, 1.97, dd) and each of C-5, C-6, and C-15, suggested that C-5 is connected to C-7 and C-15 through the fully substituted carbon C-6. HMBC correlations from H-16 to C-9 (δ_C 37.8), C-10, and C-11 and from H-11 to C-9 and C-10 indicated that C-9 is connected to C-11 and C-16 through the non-hydrogenated alkene carbon C-10. Furthermore, C-19 and C-20 (δ_C 70.7) are connected through C-18 based on HMBC correlations from H-19 to C-17, C-18, and C-20 and from H-20 (δ_H 4.54, s) to C-17, C-18, and C-19. Finally, HMBC correlations from H-20 and the acetyl methyl to the acetyl carbonyl suggested that the C-20 oxygenated methylene is acetylated. These correlations are depicted in Figure 2, and full

https://doi.org/10.1021/acs.jnatprod.3c00942
J. Nat. Prod. XXXX, XXX, XXX−XXX

Table 4. ^{1}H and ^{13}C NMR Data (500/125 MHz, CD_3OD) for Waixenicin F (7)

position	δ_C, type	δ_H (J in Hz)	COSY	key HMBC (H to C)	key ROESY
1	105.6, CH	5.21, s		3, 4, 4a	11a
3	94.5, CH	5.08, s		1, 4	5*α*, 5*β*
4	91.0, C				
4a	57.3, CH	1.67, dd (4.1, 11.2)	5*β*	3, 4, 5, 6, 11, 11a	5*α*, 6*α*, 8, 12, 19*α*
5	30.3, CH_2	*α*: 1.87, dt (3.4, 13.8)	5*β*, 6*β*	6	3, 4a, 6*α*
		β: 1.50, td (3.5, 13.4)	5*α*, 6*α*	6	3, 6*β*
6	41.4, CH_2	*α*: 1.97, m	5*β*, 6*β*	5, 7, 8	4a, 5*α*, 8
		β: 2.26, dt (3.2, 12.2)	6*α*	5	5*α*, 5*β*, 18
7	136.3, C				
8	125.9, CH	5.29, t (7.5)	6*α*, 9*β*, 18	6, 9, 19	4a, 6*α*
9	26.4, CH_2	*α*: 2.05, m	9*β*	7, 8, 10	10*α*
		β: 2.44, m	8,9*α*,10*α*,10*β*	7, 8, 10	18
10	37.4, CH_2	*α*: 2.37, dd (8.5, 12.2)	9*β*, 10*β*	9, 11, 11a, 18	9*α*, 19*β*
		β: 2.16, m	9*β*, 10*α*	9, 11, 11a, 18	11a
11	154.5, C				
11a	62.2, CH	1.79, dd, 1.0, 4.1	5*β*	1, 4a, 10, 11, 18	1, 10*β*, 18
12	127.6, CH	6.01, d (15.5)	13	4, 14	14
13	129.8, CH	6.76, dd (11.1, 15.5)	12, 14	4	16
14	128.3, CH	6.16, d (11.1)	13, 16, 17	16, 17	12, 17
15	135.1, C				
16	14.7, CH_3	1.83, s	14, 17	14, 15, 17	13
17	70.5, CH	4.56, s	14, 16	14, 15, 16, OAc-17	14
18	16.3, CH_3	1.69, s	8	6, 7, 8	6*β*, 9*β*, 11a
19	112.4, CH_2	*pro-Z*: 5.14, s	19*β*	10, 11, 11a	4a
		pro-E: 4.82, s	19*α*, 11a	10, 11a	10*α*
17-OAc	172.8, C				
	20.9, CH_3	2.07, s			

NMR assignments are compiled in Table 5. Together, these data indicate that **8** is a diterpenoid with a rare bicyclo[7.4.0]-tridecane carbon skeleton, closely related to xeniafaraunol B, where **8** is the 20-acetoxy derivative.

With the gross planar structure of compound **8** in hand, the relative configuration of compound **8** was deduced from the magnitude of $^{3}J_{H,H}$ coupling constants obtained from the ^{1}H NMR spectrum and using a ROESY experiment to determine proximity through space. The configuration of the Δ^{10} double bond is obvious based on the constraint of the ring and consistent with a ROESY correlation between H-11 (δ_H 6.41, s) and H-16 (δ_H 9.36, s). The *E* configuration of the Δ^{17} double bond was established by ROESY correlations between H-17 (δ_H 5.39) and H-20 (δ_H 4.54) and between H-19 (δ_H 1.78) and H-12 (δ_H 3.33). The absence of coupling between H-11 and H-12 suggested a ~90° dihedral angle between H-11 and H-12, which is consistent with the conformation predicted in the conformational analysis shown in Figure 2 and with a *β* orientation for H-12. The large coupling constant of ~9 Hz between H-9 (δ_H 2.82, d) and H-1 (δ_H 2.26, t), between H-1 and H-13 (δ_H 3.36, t), and between H-13 and H-12 (δ_H 3.33, m) revealed each pair is *trans* to each other. The cross peaks of H-1 with H-12 and H-8 in the ROESY spectrum indicated H-1, H-8, and H-12 were on the same side of the cyclohexene and were *β* oriented, while H-9 and H-13 were *α* oriented based on the ROESY correlations between H-9 and H-13 (δ_H 3.36, t). ROESY correlations between H-5 (δ_H 3.12, dd) and H-9*α* (δ_H 2.82, d), between H-15 and both H-14 protons, and between *pro-Z* H-14 and H-1 indicated that H-5 and H-15 were *trans* on the cyclononene ring. Accordingly, the relative configuration of the epoxide is 5*S**,6*S**. The full NMR assignments and key ROESY correlations are shown in Table 5.

Compound **8** is a diterpenoid with a bicyclo[7.4.0]tridecane carbon skeleton. Since the first natural product with a bicyclo[7.4.0]tridecane carbon skeleton was isolated from the soft coral *Efflatounaria* sp. in 1983,[50] only two other compounds possessing this ring system were reported, xeniafaraunol A and B,[51,52] and the total synthesis of (−)-xeniafaraunol A was recently reported along with (+)-waixenicin A. Compound **8**, named 20-acetoxyxeniafaraunol B, is distinct from the previously reported bicyclo[7.4.0]tridecanes by its oxygenation at C-20.

The absolute configuration of (+)-waixenicin A (**1**) was established by its recent synthesis by Magauer and co-workers,[49] and based on a putative shared biosynthesis and positive optical rotations, we assign the absolute configurations of **2**−**7** to be as drawn, consistent with that of (+)-waixenicin A. In the same report, (−)-xeniafaraunol A was synthesized from rearrangement of its corresponding xenicin under mild conditions. This confirmed the absolute configuration of the natural (−)-xeniafaraunol A, which corresponds to that drawn for **8**. Since **8** shares the same sign of specific rotation and has only minor structural modifications compared with (−)-xeniafaraunol A, we assign the absolute configuration of **8** as drawn. The demonstrated rearrangement of a xenicin to form (−)-xeniafaraunol A suggests that **8** arises from a xenicin precursor (its corresponding xenicin is **3**) either *in vivo* or during extraction and, thus, shares its biosynthetic origin with **1**, and the absolute configuration assigned to **8** matches those of shared stereogenic centers in **1** and **3**.

TRPM7-Inhbitory Activity and Structure−Activity Relationships of Waixenicin A and Analogs. In order to rank potencies of TRPM7 inhibition and assess the structure−activity relationship of a series of waixenicin A-related compounds, **1**−**8** were assayed using a well-established cell-

https://doi.org/10.1021/acs.jnatprod.3c00942
J. Nat. Prod. XXXX, XXX, XXX−XXX

Table 5. ^{1}H and ^{13}C NMR Data (500/125 MHz, CD_3OD) of 20-Acetoxyxeniafaraunol B (8)

position	δ_C, type	δ_H (J in Hz)	COSY	key HMBC (H to C)	key ROESY
1	61.4, CH	2.26, t (10.0)	9, 13	2, 3, 9, 10, 12, 13,14	8β, 12, 14β, 15
2	148.2, C				
3	27.7, CH_2	α: 2.11, m	14β	1, 2, 4, 5, 14	13, 5
		β: 2.48, m	4β, 14α, 14β	1, 2, 4, 5, 14	14α
4	28.2, CH_2	α: 2.12 m	3β, 5α	2, 3, 5, 6	14α, 15
		β: 1.53 m			
5	65.7, CH	3.12, dd (2.7, 11.5)	3α, 4	3, 4	3α, 7α, 9
6	62.1, C				
7	39.9, CH_2	α: 1.57, dd (12.0, 2.0)	8α, 8β, 15	5, 6, 8, 9,15	5, 9
		β: 1.97, dd (4.5, 12.0)	8α, 8β	5, 6, 8, 9,15	8α, 8β
8	33.3, CH_2	α: 1.65, m	7β, 9	7	7β
		β: 1.49, m	7α, 9	7	1, 7β, 15
9	37.8, CH	2.82, d (8.8)	1, 8α, 8β, 11		5, 7α, 13
10	147.9, C				
11	152.0, CH	6.41, br s	9, 12	9, 10, 12, 13, 17	16
12	45.4, CH	3.33, m	11, 13, 17	10, 13	1, 19
13	73.8, CH	3.36, t (9.1)	1, 12	12, 17	3α, 9, 17
14	119.6, CH_2	*pro-Z*: 5.16, s	3α, 3β	1, 3	1, 15
		pro-E: 5.11, s	3β	1, 3	3β, 15
15	19.5, CH_3	1.23, s	5α	5, 6, 7	7β, 8β, 14α, 14β
16	195.8, CH	9.36, s		10, 11, 9	11
17	129.5, CH	5.39, dd (1.1, 8.8)	12, 19, 20	12, 13, 19, 20	13, 20
18	135.6, C				
19	14.9, CH_3	1.79, d (1.1)	17	17, 18, 20	12
20	70.7, CH_2	4.54, s	17	17, 18, 19, 20-OAc	17
20-Ac	172.8, C				
	20.9, CH_3	2.06, s			

based cation-imaging assay that measures TRPM7 conductance.[5,6] In addition to waixenicin A (**1**), compounds **2**, **3**, **4**, and **6** showed significant inhibitory activity against the TRPM7 cation channel in the μM range (Table 6). Compounds **3**, **4**, and **6** retain activity despite variation in the nine-membered ring system. However, compounds **5**, **7**, and **8** were inactive up to 150 μM, suggesting that the 12-OAc and the dihydropyran ring system are required for TRPM7 activity. Figure 3 shows a proposed preliminary structure−activity relationship based on our data.

Table 6. Inhibition of TRPM7-Mediated Ion Channel Conductance by *Sarcothelia edmondsoni* Isolates Using the Cation Imaging Assay

compound	IC_{50} value (μM)	95% conf interval (μM)
1	20	17−23
2	12	9.3−15
3	33	27−41
4	13	9.0−17
5	>130	
6	20	16−23
7	>150	
8	>150	
2-aminoethyl diphenylborinate (2-APB)	22	9−26

The disparity between the potency in the patch-clamp versus cell-based ion conductance assays, i.e., 3 orders of magnitude, has been addressed previously and likely reflects the broader time window in the cell-based ion conductance assay (e.g., the preincubation period) for nonspecific binding of the relatively nonpolar waixenicins to media components,[6] whereas the patch-clamp experiments demonstrate the inherent potency of the compounds that are directly delivered to the cell membrane. We view these assays as complementary, as they both measure TRPM7 function; however, the patch-clamp assay more directly measures compound−protein interactions, and the cation imaging assay is able to also better reflect relevant physiochemical properties.

Waixenicin B (**2**) demonstrated the highest potency in the cation imaging assay, with an IC_{50} comparable to but consistently lower than that of waixenicin A (**1**). The increased potency may reflect a lowered log*P* for waixenicin B (**2**) based on the additional hydroxy, which would be reflected in enhanced water solubility.

The high inherent potency of waixenicin B (**2**) was confirmed in whole-cell patch-clamp experiments, which demonstrated an IC_{50} of 90 nM (Figure 4). With both compounds having strong inherent potency in the patch-clamp experiments (waixenicin A (**1**), IC_{50} = 16 nM),[6] both of these natural products may be strong starting points for lead development for TRPM7 inhibitors. The higher potency of waixenicin B (**2**) in the cell-based assay compared with waixenicin A (**1**) may also reflect higher solubility that provides waixenicin B (**2**) better bioavailability compared with waixenicin A (**1**) during the preincubation stage of the cell-based assay. Improving the pharmacokinetics and solubility of the waixenicin A (**1**) pharmacophore may be an important goal in medicinal chemistry efforts to develop the pharmacophore based on and expanding on the SAR presented here, along with conformational and structural analyses discussed in the next sections. The high inherent potency of both waixenicins A (**1**) and B (**2**) supports their use as starting points for structural optimization.

Electrophilicity and Drug-Likeness of Waixenicin A (1). Waixenicin A (**1**) possesses a high inherent potency (TRPM7 IC_{50} 16 nM) and selectivity against its intended target, has exhibited activity consistent with TRPM7 inhibition as a tool compound in numerous laboratories, and has physiochemical properties consistent with drug-likeness as illustrated by no violations among five drug-likeness filters featured in the SwissADME Web tool.[47] As a predictor of blood brain barrier permeation as needed for CNS therapeutics, the central nervous system multiparameter optimization (CNS MPO)[53] was used to score waixenicin A. The CNS MPO considers calculated log*P* and log*D*, molecular weight, total polar surface area, hydrogen bond donors, and pK_a of the conjugate acid of basic groups. Waixenicin A scored 3.8 on the CNS MPO scale using a calculated log*P* value (consensus 1-octanol−water log*P* value from SwissADME is 4.0), whereas 77% of CNS drugs have CNS MPO scores of ≥4.[53] We directly measured the partition coefficient for waixenicin A (**1**) (log*P* = 3.8, 95% confidence interval 3.62−4.15), and with the measured value the CNS MPO calculation is 4.0. Although waixenicin A (**1**) has

https://doi.org/10.1021/acs.jnatprod.3c00942
J. Nat. Prod. XXXX, XXX, XXX−XXX

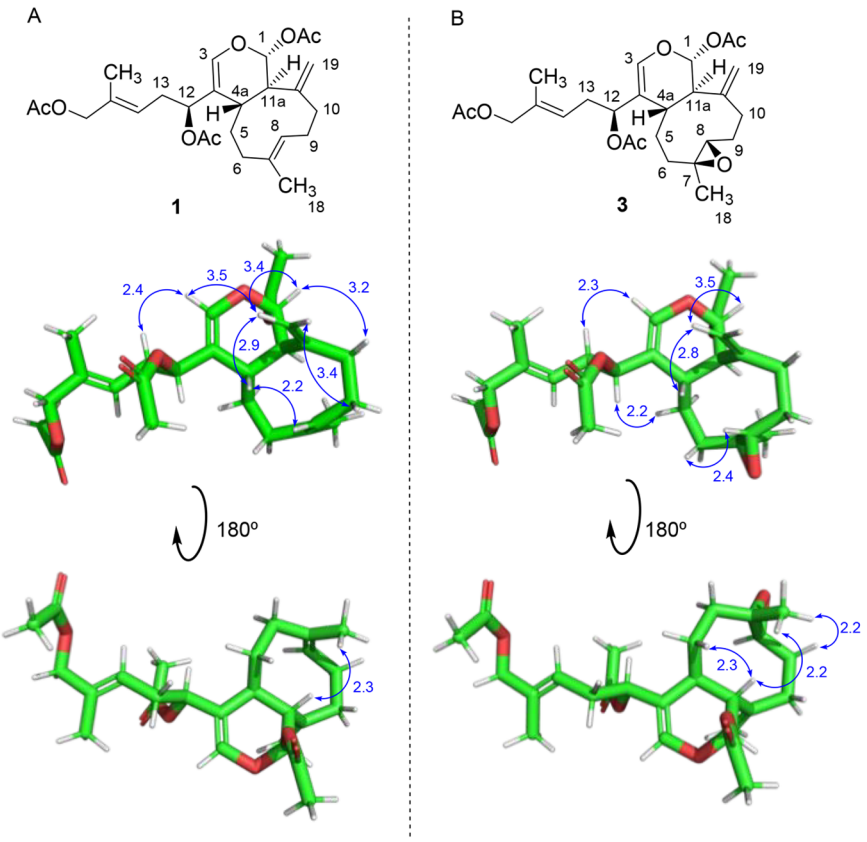

Figure 8. Observed NOE correlations (blue arrows) from ROESY experiments depicted on the lowest energy conformers of (A) waixenicin A (**1**) and (B) 7*S*,8*S*-epoxywaixenicin A (**3**). The depicted low-energy conformers and H−H distances (blue numbers in Å; determined in PyMol) were determined through DFT calculations using a methanol continuum solvation model (B3LYP/6-31G, SMD-MeOH).

demonstrated *in vivo* CNS activity in a neonatal mouse model,[17] its predicted permeation is marginal, which provides some parameters to direct structural optimizations.

We propose that waixenicin A (**1**) may be a covalent inhibitor of TRPM7. Although the electrophilicity of waixenicin A (**1**) has been discussed in the literature,[49] here we report the first evidence of irreversible inhibition of TRPM7 by waixenicin A (**1**), consistent with an electrophilic mechanism for covalent binding of the compound to its target. We applied waixenicin A (**1**) to patched cells at 10 μM for 50, 100, and 150 s (Figure 5). The inhibition of the TRPM7 current was pronounced and caused essentially full inhibition following each application for all infusion times, and no wash out of the effect was detected within the experimental time frame of 10 min. These results are consistent with irreversible and covalent inhibition. Waixenicin A possesses several structural features that could serve as latent electrophiles, and each is shared with TRPM7-active compounds **2**, **3**, **4**, and **6**, while one or both of these features are absent from the inactive compounds **5**, **7**, and **8**. Figure 6 shows two proposed mechanisms for electrophilic capture by waixenicin A and related compounds. First, loss of the 12-acetoxy group, part of a vinylogous acetal center (*vide infra*), results in a resonance-stabilized oxocarbenium ion that is electrophilic at C-3 and C-12, enabling a potential reaction with nucleophilic residues in TRPM7. Second, the substituted dihydropyran is a masked 1,5-dialdehyde that can form upon hydrolysis of the C-1 acetate and following conversion to the hemiacetal to an aldehyde and enol, which would rapidly tautomerize to the dialdehyde and can then undergo carbonyl addition and condensation reactions. Interestingly, the inactive compound **7**, the 12-deacetyl analog of waixenicin A, also possesses the masked dialdehyde but lacks the acetoxy leaving group at C-12, which would slow the generation of an oxocarbenium ion. At the same time, waixenicins C and D, which were reported previously from a hexane extract of *S. edmondsoni* that was partitioned with methanol−water,[2] are both net substitution products of methanol presumably reacting with the resonance-stabilized oxocarbenium ion that can undergo capture at C-12 or C-3, respectively. These two observations favor the substitution reaction as a potential mechanism for waixenicin A inhibition of TRPM7.

Conformational Analysis of Compounds 1, 2, 3, 7, and 8. In order to explore the overall conformation of waixenicin A and other potent analogs while also studying any potential conformational requirements of the waixenicin A pharmacophore, energy minimizations of waixenicin A (**1**), waixenicin B (**2**), and 7*S*,8*S*-epoxywaixenicin A (**3**) were performed using DFT calculations in a methanol continuum solvation model (B3LYP/6-31G, SMD-MeOH), similar to those calculated for waixenicin F (**7**) and 20-acetoxyxeniafaraunol B (**8**) (*vide infra*). Low-energy conformers were initially generated by energy minimization using Molecular Operating Environment (MOE) with solvation in methanol using the crystal structure of waixenicin B (**2**) as a reference point. Ten low-energy conformers, ranging from the lowest to the highest obtained by MOE, were then further optimized and minimized using density functional theory (B3LYP/6-31G) in a methanol continuum solvation model (SMD) utilizing Gaussian 16.[54]

https://doi.org/10.1021/acs.jnatprod.3c00942
J. Nat. Prod. XXXX, XXX, XXX−XXX

These results were then compared to NOE data obtained in CD_3OD as a H_2O mimic, to further understand the solution conformation and potential biologically relevant conformation of the rather rigid cyclononenes of these natural products. Not surprisingly, the low-energy solution conformations of xenicin diterpenes **1**, **2**, and **3** in methanol were very similar to that of waixenicin B (**2**) in the solid state based on the single-crystal X-ray structure reported by Coval (Figure 7A).[1] Furthermore, an overlay of the two lowest energy conformers identified for waixenicin A (**1**) only showed minor variation in the side-chain, and the two low-energy conformers, with differences primarily in the more flexible side-chain as expected, had nearly identical energies. These results support the idea that the bicyclic ring structure is relatively rigid, while the bis-acetoxy side-chain shows some flexibility beyond the C-12 acetoxy group (*vide infra*) in methanol (Figure 7B). Very similar observations were made for 7*S*,8*S*-epoxywaixenicin A (**3**); the 10 low-energy conformers identified had nearly identical conformations except for the side-chain beyond the C-12 acetoxy group (Figure 7C).

The rigidity and overall topology of the bicyclic cyclononene−dihydropyran sector of these natural products were also corroborated by the presence of key transannular NOE interactions identified through ROESY experiments. The observed ROESY interactions were analyzed and compared to H−H distances observed for the lowest energy conformer found through DFT calculations (Figure 8). As expected, ROESY correlations found in waixenicin A (**1**) and 7*S*,8*S*-epoxywaixenicin A (**3**) were similar, indicating that the major conformational rotamer of the cyclononene places the C-18 vinyl methyl and C-11a methine proton in close proximity (Figure 8A). Additionally, interactions between the cyclononene exocyclic alkene hydrogens, H-19 (δ 4.78), and the dihydropyran ring hydrogens, H-1 (δ 5.81), H-3 (δ 6.53), and H-4a (δ 2.17), reveal that the exocyclic C-11/C-19 alkene adopts a conformation that places it in close proximity and in a nearly orthogonal relationship to the dihydropyran ring.

In the case of 7*S*,8*S*-epoxywaixenicin A (**3**), observed NOE correlations were similar to those of waixenicin A (**1**) with some exceptions (Figure 8B). The correlations between H-19 (δ 4.89) and H-3 (δ 6.56), between H-19 (δ 5.05) and H-9 (δ 2.22), and between H-8 (δ 2.99) and H-4a (δ 2.25) are absent. The rotational conformer shown is supported by the presence of NOE correlations between H-8 and H-6 (δ 1.14), H-18 (δ 1.33) and H-9, and also H-11a (δ 2.45) and H-5 (δ 2.12). These NOE correlations provide evidence for the rotational conformer depicted for the cyclononene of waixenicin A (**1**) and 7*S*,8*S*-epoxywaixenicin A (**3**), which is the same for these two compounds. The observed ROESY correlations are also consistent with the conformation of the waixenicin B (**2**) observed in the X-ray crystal structure (Figure 7A), indicating close correlation between the solid and solution state for these overall rather rigid molecules.

As previously described by Corey,[55] even simplified cyclononenes bearing two alkenes and a vinyl methyl group related to those found in the caryophylloid family, which includes the waixenicins, possess conformational chirality due to unfavorable transannular interactions during interconversion. In the case of waixenicin A (**1**), a single conformer is observed for the cyclononene in the natural product in both the solid state (X-ray) and solution state (NMR in CD_3OD) based on our studies (Figure 9A). Although the energy difference between these conformational isomers is quite low (~2 kcal/mol, DFT), a high energy barrier likely precludes facile interconversion at ambient

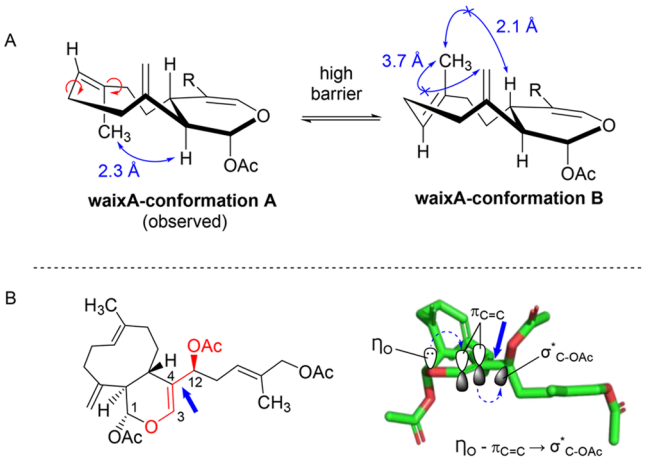

Figure 9. (A) Noninterchangeable (at ambient temperature) natural and unnatural conformers of waixenicin A (**1**) involving rotation around the allylic bonds (red arrows; side-chain presented as R for clarity). The major conformer was supported by NOE correlations (blue double-headed arrows) observed and not observed with the low-energy conformer obtained through DFT calculations (B3LYP/6-31G, SMD-MeOH). (B) A potential vinylogous hyperconjugation effect impacting the lowest energy conformer about the C-4/C-12 bond (blue bold arrow) of the waixenicin A (**1**) side-chain.

temperatures. These NOE correlations support the lowest energy rotational conformers of the cyclononene found via DFT calculations. In the case of waixenicin A (**1**), this cyclononene conformation exposes the *si* face of the C-7/C-8 alkene, leading to peripheral attack and the observed single epoxide diastereomer obtained through air oxidation leading to 7*S*,8*S*-epoxywaixenicin A (**3**). This conformational isomerism was previously observed in synthetic studies by Corey toward caryophylloids[51] and more recently by Maguer in his synthesis of waixenicin A (**1**).[49] We anticipate that many members of the caryophyllene terpene family bearing related cyclononene rings will possess such conformational isomerism. Furthermore, these conformations may correspond to the bioactive conformations of the waixenicins.

Our DFT calculations also reveal a striking conformational preference of the C-12 acetoxy group of waixenicin A (**1**), leading to a preferred conformation about the C-4/C-12 bond of the side-chain of waixenicins A and B. Interestingly, this C-4/C-12 conformational preference is also observed in the waixenicin B (**2**) crystal structure (see Figure 7). We attribute this conformational preference to a vinylogous hyperconjugation effect, an "anomeric-like" effect,[52] that extends from the dihydropyran oxygen to the C-12 acetoxy group (Figure 9B). In the present case, the lone pair of the dihydropyran oxygen is aligned to donate into the π-system of the alkene, in turn donating electron density to the σ^* of the C-12 acetoxy group ($n_O - p_{C=C} \rightarrow \sigma^*_{C-O}$). We posit that this stabilizing effect contributes to the observed, preferred conformation of the waixenicin A (**1**) side-chain about the C-4/C-12 bond and likely is present in other members of this family. In the case of both waixenicin A (**1**) and 7*S*,8*S*-epoxywaixenicin A (**2**), the dihedral angle between the π-system of the dihydropyran and the C-12 acetoxy group is ~70° for both observed low-energy side-chain conformers (Figure 7B,C), which may be a compromise from the ideal ~90° dihedral angle to minimize $A^{1,3}$-interactions. Furthermore, natural bond orbital (NBO) analysis[56] performed on the lowest energy conformer of waixenicin A (**1**) supports

https://doi.org/10.1021/acs.jnatprod.3c00942
J. Nat. Prod. XXXX, XXX, XXX−XXX

this stabilizing interaction due to a vinylogous hyperconjugation effect and also the observed C-4/C-12 conformations in these natural products (see the SI for further details, Figure S34).

Conclusions. The TRPM7 ion channel is emerging as a potential drug target for ischemic diseases and certain cancers. At the same time, the waixenicin A pharmacophore, with nanomolar potency in patch-clamp studies and no effect on related channels including the closest homologue TRPM6, demonstrates the inherent selectivity and potency for TRPM7 needed for a successful drug lead. As such, the SAR reported herein employing novel xenicane diterpenes and the conformational analyses also described can serve as a starting point for the full synthesis or semisynthesis of improved inhibitors of the TRPM7 ion channel. This preliminary SAR begins to define the essential structural features required for TRPM7 inhibition by the waixenicin A pharmacophore, and both the structural elements associated with activity and the *in vitro* bioassay data presented here support the hypothesis that waixenicin A inhibits TRPM7 activity through a covalent mechanism. The rigidity of the bicyclic dihydropyran−cyclononene core and the vinylogous anomeric effect begin to define possible structural requirements for bioactivity. These insights into the structural and conformational requirements for activity are informing our ongoing medicinal chemistry efforts to develop waixenicin A derivatives as TRPM7 inhibitors with improved pharmacokinetics for subsequent drug lead development.

EXPERIMENTAL SECTION

General Experimental Procedures. The optical rotation was measured on a Rudolph Research AUTOPOL III polarimeter. The UV spectra were recorded on a PerkinElmer Lambda 20 spectrophotometer. The IR spectra were recorded on a PerkinElmer Spectrum RX1 FTIR spectrometer. The NMR experiments were performed on a Varian 500 spectrometer operating at 500 and 125 MHz, for ^{1}H and ^{13}C, respectively, or a Varian 300 spectrometer operating at 300/75 MHz. Samples were dissolved in CD_3OD, using the residual CHD_2OD signal (δ_H 3.31 ppm) as an internal standard for ^{1}H NMR and CD_3OD (δ_C 49.15 ppm) for ^{13}C NMR. High-accuracy mass spectrometric data were obtained on an Agilent 6530 Q-TOF using ESI ionization; low-accuracy mass spectrometric data were obtained on a Thermo Finnigan LCQ Deca XP Max using ESI mode.

Animal Material. The soft coral *S. edmondsoni* was collected by hand in 2−4 m depth in waters adjacent to Lanikai Beach, on the island of Oahu, Hawaii, on March 3 and December 14, 2007. Samples were frozen and freeze-dried. The soft coral was identified as *S. edmondsoni* by Dr. Samuel Kahng (Hawaii Pacific University). A voucher sample (030307-LAN-1) is preserved in 4% formaldehyde and stored in the Department of Natural Science, Hawaii Pacific University.

Extraction and Isolation. The freeze-dried soft coral biomass (80.1 g) was extracted with CH_2Cl_2−methanol (4:1) (1 L × 3) at room temperature to yield 9.33 g of dark green residue. The organic extract was subjected to MPLC over silica gel using multiple step gradients from *n*-hexane−acetone (100:1) to acetone and then from CH_2Cl_2−methanol (10:1) to 100% methanol, resulting in 22 fractions. The fraction that eluted with *n*-hexane−acetone (20:1) was fractionated (in several portions) by reversed-phase HPLC (Phenomenex Luna C18(2), 10 μm, 21.2 × 250 mm) with an MeCN−H_2O gradient (50−100% MeCN over 50 min; flow rate: 7.6 mL/min; UV detection: 210 nm) to get the major component **1** (261 mg, t_R 40.0 min) and minor components **8** (0.8 mg, t_R 23.4 min), **3** (26 mg, t_R 28.1 min), and **7** (1.0 mg, t_R 32.1 min). The MPLC fraction eluted with *n*-hexane−acetone (8:1) was also fractionated by reversed-phase HPLC (Phenomenex Luna C18(2), 5 μm, 10.0 × 250 mm) with a MeCN−H_2O gradient (30−100% MeCN over 50 min; flow rate: 3.8 mL/min; UV detection: 210 nm) to yield compound **6** (4.8 mg, t_R 33.5 min). The MPLC fraction eluted with *n*-hexane−acetone (5:1) was fractionated using the previous reversed-phase HPLC conditions to yield compound **5** (3.6 mg, t_R 32.4 min). The MPLC fraction eluted with *n*-hexane−acetone (4:1) was fractionated, also using the previous reversed-phase HPLC conditions, to give compounds **4** (1.0 mg, t_R 21.5 min) and **2** (2.0 mg, t_R 30.5 min).

7*S*,8*S*-Epoxywaixenicin A (3): colorless oil; $[\alpha]^{27}_D$ +33 (*c* 0.049, MeOH); UV (MeOH) λ_{max} (log ε) 202 (4.09), 236 (3.43), 277 (3.36) nm; IR (film on AgCl plate) ν_{max} 2936, 2858, 1733, 1650, 1449, 1370, 1233, 1150, 1042 cm^{-1}; ^{1}H and ^{13}C NMR data (CD_3OD), see Tables 1 and 2; (+)-ESIMS *m*/*z* 477 $[M + H]^+$, 494 $[M + NH_4]^+$, 499 $[M + Na]^+$; (+)-HRESIMS *m*/*z* 417.2273 $[M - AcOH + H]^+$ (calcd for $C_{24}H_{33}O_6^+$, 417.2272; +0.2 ppm), 477.24683 $[M + H]^+$ (calcd for $C_{26}H_{37}O_8^+$, 477.2483; 0.0 ppm), 499.2301 $[M + Na]^+$ (calcd for $C_{26}H_{36}O_8Na^+$, 499.2302; Δ −0.2 ppm).

7*S*,8*S*-Epoxywaixenicin B (4): colorless oil; $[\alpha]^{27}_D$ +38 (*c* 0.34, MeOH); UV (MeOH) λ_{max} (log ε) 207 (4.00) 240 (3.67), 274 (3.17) nm; IR (film on AgCl plate) ν_{max} 2935, 1734, 1454, 1372, 1230, 1143, 1021, 954 cm^{-1}; ^{1}H and ^{13}C NMR data (CD_3OD), see Tables 1 and 2; (+)-ESIMS *m*/*z* 510 $[M + NH_4]^+$, 556 $[M + CH_3CN + Na]^+$; (+)-HRESIMS *m*/*z* 433.2216 $[M - AcOH + H]^+$ (calcd for $C_{24}H_{33}O_7^+$, 433.2221; −1.2. ppm), 515.2246 $[M + Na]^+$ (calcd for $C_{26}H_{36}O_9Na^+$, 515.2252; Δ −21.2 ppm).

12-Deacetylwaixenicin A (5): colorless oil; $[\alpha]^{28}_D$ +67 (*c* 0.26, MeOH); UV (MeOH) λ_{max} (log ε) 205 (4.14), 240 (3.50), 274 (3.22) nm; IR (film on AgCl plate) ν_{max} 3456, 2927, 2857, 1734, 1659, 1450, 1375, 1235, 1150, 1020, 950 cm^{-1}; ^{1}H and ^{13}C NMR data (CD_3OD), see Table 3; (+)-ESIMS *m*/*z* 436 $[M + NH_4]^+$, 441 $[M + Na]^+$; (+)-HRESIMS *m*/*z* 441.2247 $[M + Na]^+$ (calcd for $C_{24}H_{34}O_6Na^+$, 441.2248; −0.2 ppm).

Waixenicin E (6): colorless oil; $[\alpha]^{27}_D$ +22 (*c* 0.33, MeOH); UV (MeOH) λ_{max} (log ε) 204 (4.43) 238 (4.08), 276 (3.82) nm; IR (film on AgCl plate) ν_{max} 2935, 1734, 1438, 1367, 1230, 1148, 1016, 960 cm^{-1}; ^{1}H and ^{13}C NMR data (CD_3OD), see Table 3; (+)-ESIMS *m*/*z* 536 $[M + NH_4]^+$, 541 $[M + Na]^+$; (+)-HRESIMS *m*/*z* 541.2413 $[M + Na]^+$ (calcd for $C_{28}H_{38}O_9Na^+$, 541.2408; +0.9 ppm).

Waixenicin F (7): colorless oil; $[\alpha]^{26}_D$ +19 (*c* 0.16, MeOH); UV (MeOH) λ_{max} (log ε) 238 (4.16) nm; IR (film on AgCl plate) ν_{max} 3378, 2925, 2848, 1733, 1634, 1454, 1370, 1228 cm^{-1}; ^{1}H and ^{13}C NMR data (CD_3OD), see Table 4; (+)-ESIMS *m*/*z* 357 $[M + H - H_2O]^+$, 375 $[M + H]^+$, 392 $[M + NH_4]^+$, 397 $[M + Na]^+$; (+)-HRESIMS *m*/*z* 297.1851 $[M - H_2O - CH_3COOH + H]^+$ (calcd for $C_{20}H_{25}O_2^+$, 297.1849; +0.7 ppm), 357.2060 $[M - H_2O + H]^+$ (calcd for $C_{22}H_{29}O_4^+$, 357.2060; 0.0 ppm), 397.1986 $[M + Na]^+$ (calcd for $C_{22}H_{30}O_5Na^+$, 397.1985; +0.3 ppm), 771.4069 $[2M + Na]^+$ (calcd for $C_{44}H_{60}O_{10}Na^+$, 771.4079; −1.3 ppm)

20-Acetoxyxeniafaraunol B (8): colorless oil; $[\alpha]^{28}_D$ −17 (*c* 0.15, MeOH); UV (MeOH) λ_{max} (log ε) 202 (3.93) 233 (3.90), 274 (3.32) nm; IR (film on AgCl plate) ν_{max} 3445, 2932, 2860, 1730, 1678, 1632, 1452, 1385, 1236, 1150, 1026, 855 cm^{-1}; ^{1}H and ^{13}C NMR data (CD_3OD), see Table 5; (−)-ESIMS *m*/*z* 409.2/411.2 $[M + Cl]^-$, 419.2 $[M + HCOO]^-$; (+)-HRESIMS *m*/*z* 397.1989 $[M + Na]^+$ (calcd for $C_{22}H_{30}O_5Na^+$, 397.1985; +1.0 ppm).

Log*P* Measurement. Waixenicin A (**1**) (15.0 mg) was dissolved in 30 mL of 1-octanol. The solution was combined with 30 mL of type 1 H_2O in a separatory funnel. After mixing, the aqueous layer was separated and 10 mL of the aqueous phase was extracted using 5 mL of dichloromethane (3 times). After drying with anhydrous $MgSO_4$, dichloromethane and 1-octanol solutions were filtered and solvents evaporated under vacuum. The experiment was conducted 3 times. LC-MS analysis was conducted on each sample residue by reconstituting each in 1.0 mL of methanol [LC-MS conditions: instrument: Agilent QTOF; injection volume: 10 μL; column: Agilent Eclipse C18 2.1 mm × 50 mm with particle size 3.5 μm; column temperature: 40 °C; solvent A: H_2O with 0.1% formic acid, solvent B: acetonitrile with 0.1% formic acid; gradient: 5% to 100% solvent B over 0−8 min, 100% B over 8−14 min; flow rate: 0.4 mL/min]. An LC-MS calibration curve was prepared with 5−7 concentration points, and the curve was fit to a polynomial equation and used to calculate the amount of waixenicin A on column for each analysis. Log*P* was calculated by taking the log of the ratio of $[\text{waixenicin A}]_{1\text{-octanol}}/[\text{waixenicin A}]_{water}$.

https://doi.org/10.1021/acs.jnatprod.3c00942
J. Nat. Prod. XXXX, XXX, XXX−XXX

TRPM7 Inhibition Assay. The TRPM7 assay used was previously published[6] and is described here briefly. Human embryonic kidney cells (HEK-293) transfected with the FLAG-murine TRPM7/pCDNA4/TO[7] (TRPM7-HEK) were provided by Dr. Andrew Scharenberg's laboratory. Cells were grown in 150 cm^2 culture flasks (Techno Plastic Products) with Dulbecco's modified Eagle's medium (DMEM, Mediatech), supplemented with 10% fetal bovine serum, 5 μg/mL blasticidin (Invitrogen), and 400 μg/mL zeocin (Invitrogen) in a humidified incubator (5% CO_2, 37 °C).

Divalent cation conductance through TRPM7 channels was measured using an established assay[6] that measures the decrease in fluorescence resulting from the extracellular addition of Mn^{2+} to TRPM7-HEK cells loaded with the Ca^{2+}-indicator dye fura-2, which is strongly bound and quenched by Mn^{2+}. TRPM7-HEK cells (50,000−60,000 cells/well) were plated in poly-L-lysine-coated 96-well plates, and TRPM7 expression was induced 2−3 h postplating by the addition of 2 μg/mL tetracycline. The culture medium was completely removed at 16−20 h postinduction and replaced with the fura-2 loading buffer: 2 μM fura-2-acetoxymethyl ester (Invitrogen), 0.10% pluronic, and 2.0 mM probenicid (Sigma) in Krebs-Ringer-HEPES (KRH) buffer (135 mM NaCl, 5 mM KCl, 1.5 mM $MgCl_2$, 1.5 mM $CaCl_2$, 20 mM HEPES, and 5.6 mM glucose). Following incubation (45 min at 37 °C), the loading buffer was removed, and the cells were washed once with KRH before addition of KRH as the assay buffer. The plates were then transferred to a prewarmed (37 °C) FlexStation 3 (Molecular Devices). Cells were initially incubated with compounds (5 or 6 concentrations of 3-fold serial dilutions in triplicate) or vehicle for ∼15 min. In all assays performed, vehicle-receiving, induced TRPM7-HEK cells served as vehicle control for the activation of a TRPM7-mediated Mn^{2+} influx, while wells containing either parental HEK cells (receiving vehicle) or uninduced TRPM7-HEK served as negative controls to define the background for the changes of cytosolic $[Mn^{2+}]$. The Ca^{2+}-independent fluorescence (excitation 360 nm; emission 510 nm) of fura-2 was monitored for 90 s following the addition of 10 mM $MnCl_2$. The flux of Mn^{2+} was taken as the maximum slope of the change in fluorescence following $MnCl_2$ addition. Data were normalized by expressing the background-corrected maximum slope for each well as a percent of the slope for background-corrected vehicle control wells (% vehicle). Assays were repeated on separate days, and the pooled data were fitted to a dose−response curve with Prism statistical software (GraphPad Software, version 5.01; log of inhibitor concentration vs normalized response, variable slope). The nonselective ion channel inhibitor 2-aminoethyl diphenylborinate (Sigma) served as a positive control in each assay. Calculated IC_{50} values and 95% confidence intervals are shown in Table 6.

Electrophysiology. Tetracycline (Tet)-inducible HEK293-TREx cells, stably transfected with human TRPM7,[S7] were cultured in DMEM medium (Gibco) containing 10% fetal bovine serum (FBS, Gibco), zeocin (0.4 mg/mL, Invitrogen), and blasticidin (5 μg/mL, Invitrogen). Overexpression was induced by adding 1 μg/mL tetracycline (Gibco) to the culture medium. Patch-clamp experiments were performed 18−22 h post-tetracycline induction. For whole-cell patch-clamp experiments assessing overexpressed human TRPM7, the extracellular solution contained (in mM) 140 NaCl, 2.8 KCl, 2 $MgCl_2$, 1 $CaCl_2$, 10 HEPES-NaOH, and 11 glucose (pH 7.2, 300 mOsm). Intracellular pipet-filling solutions contained (in mM) 130 Cs-glutamate, 8 NaCl, 1 $MgCl_2$, 10 Cs-BAPTA, and 10 HEPES-CsOH (pH 7.2, 300 mOsm). All salts were purchased from Sigma. Waixenicin A (**1**) was dissolved in methanol and then diluted to a final concentration of 10 μM for the extracellular solution used for patch-clamp experiments. As a vehicle control application, appropriate methanol was added to the extracellular solution. Patch-clamp experiments were performed in the whole-cell configuration using an EPC-9 amplifier (HEKA, Germany). hTRPM7 currents were elicited by voltage ramps of −100 mV to +100 mV from a holding potential of 0 mV over 50 ms and acquired at 0.5 Hz. Current amplitudes over the course of the experiment were extracted at −80 mV and +80 mV and plotted versus time. Data were normalized to the time point before compound application. All values are given as mean and standard error of the mean (SEM). Patch glass pipettes (Sutter Instrument) were pulled and heat polished and had a tip resistance of 2−3 MΩ with the solutions used.

Calculations. Low-energy conformers were initially generated by energy minimization using MOE with solvation in methanol. Ten low-energy conformers, ranging from the lowest to the highest energies obtained by MOE, were then further optimized and minimized using density functional theory (B3LYP/6-31G) in a methanol continuum solvation model (SMD). Analysis of the resulting structures was performed using Gaussian and PyMOL. Structures shown were generated in PyMOL.

■ ASSOCIATED CONTENT

Supporting Information

The Supporting Information is available free of charge at https://pubs.acs.org/doi/10.1021/acs.jnatprod.3c00942.

One- and two-dimensional NMR spectra of compounds **1**−**3**; one-dimensional NMR spectra of compounds **4**−**8**; mass spectra for compounds **1**−**8**; DFT calculation data; NBO analysis of **1**; list of FIDs included in the Supporting Information zipped NMR data folder (PDF)

Raw NMR data for compounds **1**−**8** (ZIP)

■ AUTHOR INFORMATION

Corresponding Authors

Daniel Romo − *Department of Chemistry & Biochemistry, Baylor University, Waco, Texas 76798-7348, United States;* orcid.org/0000-0003-3805-092X; Phone: (254) 710-7075; Email: Daniel_Romo@baylor.edu

Andrea Fleig − *Laboratory of Cell and Molecular Signaling, Center for Biomedical Research at The Queen's Medical Center, Honolulu, Hawaii 96813, United States; Cancer Biology Program, University of Hawaii Cancer Center and Department of Cell and Molecular Biology, John A. Burns School of Medicine at the University of Hawaii, Honolulu, Hawaii 96813, United States*; Phone: (808) 691-7931; Email: afleig@hawaii.edu

F. David Horgen − *Chemistry and Biochemistry, Hawaii Pacific University, Kaneohe, Hawaii 96744, United States;* orcid.org/0000-0001-9409-3030; Phone: (808) 236-5864; Email: dhorgen@hpu.edu

Authors

Guangmin Yao − *Hubei Key Laboratory of Natural Medicinal Chemistry and Resource Evaluation, School of Pharmacy, Tongji Medical College, Huazhong University of Science and Technology, Wuhan 430030, People's Republic of China; Chemistry and Biochemistry, Hawaii Pacific University, Kaneohe, Hawaii 96744, United States*

Matthew R. Parris − *Department of Chemistry & Biochemistry, Baylor University, Waco, Texas 76798-7348, United States*

W. Cedric Kuo − *Chemistry and Biochemistry, Hawaii Pacific University, Kaneohe, Hawaii 96744, United States*

Peter Pörzgen − *Chemistry and Biochemistry, Hawaii Pacific University, Kaneohe, Hawaii 96744, United States*

Brandi Castillo − *Chemistry and Biochemistry, Hawaii Pacific University, Kaneohe, Hawaii 96744, United States*

Evan S. Mason − *Department of Chemistry & Biochemistry, Baylor University, Waco, Texas 76798-7348, United States*

Andres Chinchilla − *Department of Chemistry & Biochemistry, Baylor University, Waco, Texas 76798-7348, United States*

Junhao Huang − *Laboratory of Cell and Molecular Signaling, Center for Biomedical Research at The Queen's Medical Center, Honolulu, Hawaii 96813, United States;* Present

https://doi.org/10.1021/acs.jnatprod.3c00942
J. Nat. Prod. XXXX, XXX, XXX−XXX

Address: Department of Sports and Health, Guangzhou Sport University, Guangzhou, 510500, China
Sayuri Suzuki − *Laboratory of Cell and Molecular Signaling, Center for Biomedical Research at The Queen's Medical Center, Honolulu, Hawaii 96813, United States*
Rylee Ross − *Chemistry and Biochemistry, Hawaii Pacific University, Kaneohe, Hawaii 96744, United States*
Ellis Akana − *Chemistry and Biochemistry, Hawaii Pacific University, Kaneohe, Hawaii 96744, United States*
Savana Vander Schuit − *Chemistry and Biochemistry, Hawaii Pacific University, Kaneohe, Hawaii 96744, United States*
Steven P. Miller − *Department of Pediatrics, University of British Columbia and BC Children's Hospital, Vancouver, British Columbia V6H 3N1, Canada*
Reinhold Penner − *Laboratory of Cell and Molecular Signaling, Center for Biomedical Research at The Queen's Medical Center, Honolulu, Hawaii 96813, United States; Cancer Biology Program, University of Hawaii Cancer Center and Department of Cell and Molecular Biology, John A. Burns School of Medicine at the University of Hawaii, Honolulu, Hawaii 96813, United States*
Hong-Shuo Sun − *Department of Surgery and Department of Physiology, Faculty of Medicine, University of Toronto, Toronto, Ontario M5S 1A8, Canada*
Zhong-Ping Feng − *Department of Physiology, Faculty of Medicine, University of Toronto, Toronto, Ontario M5S 1A8, Canada*
Kenneth G. Hull − *Department of Chemistry & Biochemistry, Baylor University, Waco, Texas 76798-7348, United States; The Baylor Synthesis and Drug-Lead Discovery Laboratory, Baylor University, Waco, Texas 76798, United States;* orcid.org/0000-0002-3697-9551

Complete contact information is available at: https://pubs.acs.org/10.1021/acs.jnatprod.3c00942

Author Contributions

G.Y. and M.R.P. contributed equally to the manuscript.

Notes

The authors declare no competing financial interest.

■ ACKNOWLEDGMENTS

This project was supported in part by grants P20 GM103466 from the National Institute of General Medical Sciences (to F.D.H.), R61 NS124922 from the National Institute of Neurological Disorders and Stroke (to D.R., Z.-P.F., A.F., F.D.H., K.G.H., H.-S.S., S.M.), and R01AT011162 (to R.P.) from the National Center for Complementary and Integrative Health, each of the National Institutes of Health, Bethesda, MD, USA. The content is solely the responsibility of the authors and does not necessarily represent the official views of the National Institutes of Health. Additional support was provided by the American Society of Pharmacognosy through an ASP Undergraduate Research Award to C.W.K. and by a grant from Hamamatsu/Queen's PET Imaging, LLC (S.S., A.F.). We also thank Dr. S. Kahng (Hawaii Pacific University) for identifying the soft coral, Ms. T. Vansach for conducting accurate MS analyses, and Mr. W. Yoshida (University of Hawaii at Manoa) for performing the high-field NMR experiments.

■ REFERENCES

(1) Devaney, D. M. In *Reef and Shore Fauna of Hawaii, Section 1: Protozoa through Ctenophora*; Bishop Museum: Honolulu, 1977; pp 119−129.
(2) Cooray, N. M. *Chemical Investigations of Three Marine Invertebrates*; University of Hawaii at Manoa, Honolulu, HI, 1989.
(3) Coval, S. J.; Scheuer, P. J.; Matsumoto, G. K.; Clardy, J. *Tetrahedron* **1984**, *40* (19), 3823−3828.
(4) Adams, B.; Pörzgen, P.; Pittman, E.; Yoshida, W. Y.; Westenburg, H. E.; Horgen, F. D. *J. Nat. Prod.* **2008**, *71* (5), 750−754.
(5) Castillo, B.; Pörzgen, P.; Penner, R.; Horgen, F. D.; Fleig, A. *J. Biomol. Screen.* **2010**, *15* (5), 498−507.
(6) Zierler, S.; Yao, G.; Zhang, Z.; Kuo, W. C.; Porzgen, P.; Penner, R.; Horgen, F. D.; Fleig, A. *J. Biol. Chem.* **2011**, *286* (45), 39328−39335.
(7) Nadler, M. J.; Hermosura, M. C.; Inabe, K.; Perraud, A. L.; Zhu, Q.; Stokes, A. J.; Kurosaki, T.; Kinet, J. P.; Penner, R.; Scharenberg, A. M.; Fleig, A. *Nature* **2001**, *411* (6837), 590−595.
(8) Jiang, J.; Li, M.-H.; Inoue, K.; Chu, X.-P.; Seeds, J.; Xiong, Z.-G. *Cancer Res.* **2007**, *67* (22), 10929−10938.
(9) Guilbert, A.; Gautier, M.; Dhennin-Duthille, I.; Haren, N.; Sevestre, H.; Ouadid-Ahidouch, H. *Am. J. Physiol.-Cell Physiol.* **2009**, *297* (3), C493−C502.
(10) Kim, B. J.; Park, E. J.; Lee, J. H.; Jeon, J.-H.; Kim, S. J.; So, I. *Cancer Sci.* **2008**, *99* (12), 2502−2509.
(11) Wong, R.; Gong, H.; Alanazi, R.; Bondoc, A.; Luck, A.; Sabha, N.; Horgen, F. D.; Fleig, A.; Rutka, J. T.; Feng, Z.-P.; Sun, H.-S. *Cell Calcium* **2020**, *92*, No. 102307.
(12) Cordier, C.; Prevarskaya, N.; Lehen'kyi, V. *Cancers* **2021**, *13* (24), 6322.
(13) (a) Jiang, H.; Tian, S.-L.; Zeng, Y.; Li, L.-L.; Shi, J. *Brain Res. Bull.* **2008**, *76* (1−2), 124−130. (b) Chen, W.; Xu, B.; Xiao, A.; Liu, L.; Fang, X.; Liu, R.; Turlova, E.; Barszczyk, A.; Zhong, X.; Sun, C. L. F.; Britto, L. R. G.; Feng, Z.-P.; Sun, H.-S. *Mol. Brain* **2015**, *8* (1), No. 11.
(14) Arundine, M.; Tymianski, M. *Cell Calcium* **2003**, *34* (4−5), 325−337.
(15) Aarts, M.; Iihara, K.; Wei, W.-L.; Xiong, Z.-G.; Arundine, M.; Cerwinski, W.; MacDonald, J. F.; Tymianski, M. *Cell* **2003**, *115* (7), 863−877.
(16) Sun, H.-S.; Jackson, M. F.; Martin, L. J.; Jansen, K.; Teves, L.; Cui, H.; Kiyonaka, S.; Mori, Y.; Jones, M.; Forder, J. P.; Golde, T. E.; Orser, B. A.; MacDonald, J. F.; Tymianski, M. *Nat. Neurosci.* **2009**, *12* (10), 1300−1307.
(17) Turlova, E.; Wong, R.; Xu, B.; Li, F.; Du, L.; Habbous, S.; Horgen, F. D.; Fleig, A.; Feng, Z.-P.; Sun, H.-S. *Transl. Stroke Res.* **2021**, *12*, 164.
(18) Sun, H.-S.; Horgen, F. D.; Romo, D.; Hull, K. G.; Kiledal, S. A.; Fleig, A.; Feng, Z.-P. *Acta Pharmacol. Sin.* **2020**, *41*, 1519.
(19) Sun, Y.; Sukumaran, P.; Schaar, A.; Singh, B. B. *Channels Austin Tex* **2015**, *9* (5), 253−261.
(20) Lin, J.; Xiong, Z.-G. *Int. J. Physiol. Pathophysiol. Pharmacol.* **2017**, *9* (6), 211−216.
(21) Runnels, L. W.; Yue, L.; Clapham, D. E. *Science* **2001**, *291* (5506), 1043−1047.
(22) Hanano, T.; Hara, Y.; Shi, J.; Morita, H.; Umebayashi, C.; Mori, E.; Sumimoto, H.; Ito, Y.; Mori, Y.; Inoue, R. *J. Pharmacol. Sci.* **2004**, *95* (4), 403−419.
(23) Chen, H.-C.; Xie, J.; Zhang, Z.; Su, L.-T.; Yue, L.; Runnels, L. W. *PLoS ONE* **2010**, *5* (6), No. e11161.
(24) Kerschbaum, H. H.; Kozak, J. A.; Cahalan, M. D. *Biophys. J.* **2003**, *84* (4), 2293−2305.
(25) Monteilh-Zoller, M. K.; Hermosura, M. C.; Nadler, M. J. S.; Scharenberg, A. M.; Penner, R.; Fleig, A. *J. Gen. Physiol.* **2003**, *121* (1), 49−60.
(26) Parnas, M.; Peters, M.; Dadon, D.; Lev, S.; Vertkin, I.; Slutsky, I.; Minke, B. *Cell Calcium* **2009**, *45* (3), 300−309.
(27) Chubanov, V.; Mederos y Schnitzler, M.; Meißner, M.; Schäfer, S.; Abstiens, K.; Hofmann, T.; Gudermann, T. *Br. J. Pharmacol.* **2012**, *166* (4), 1357−1376.

(28) Strøbæk, D.; Hougaard, C.; Johansen, T. H.; Sørensen, U. S.; Nielsen, E. Ø.; Nielsen, K. S.; Taylor, R. D. T.; Pedarzani, P.; Christophersen, P. *Mol. Pharmacol.* **2006**, *70* (5), 1771−1782.
(29) Rössig, A.; Hill, K.; Nörenberg, W.; Weidenbach, S.; Zierler, S.; Schaefer, M.; Gudermann, T.; Chubanov, V. *Cell Calcium* **2022**, *106*, No. 102640.
(30) Chubanov, V.; Gudermann, T. *Int. J. Mol. Sci.* **2020**, *21* (19), 7017.
(31) Suzuki, S.; Penner, R.; Fleig, A. *Sci. Rep.* **2020**, *10* (1), 2333.
(32) Suzuki, S.; Fleig, A.; Penner, R. *Sci. Rep.* **2023**, *13* (1), 6341.
(33) Brinkmann, V.; Billich, A.; Baumruker, T.; Heining, P.; Schmouder, R.; Francis, G.; Aradhye, S.; Burtin, P. *Nat. Rev. Drug Discovery* **2010**, *9* (11), 883−897.
(34) Qin, X.; Yue, Z.; Sun, B.; Yang, W.; Xie, J.; Ni, E.; Feng, Y.; Mahmood, R.; Zhang, Y.; Yue, L. *Br. J. Pharmacol.* **2013**, *168* (6), 1294−1312.
(35) Schlecht, R.; Scholz, S. R.; Dahmen, H.; Wegener, A.; Sirrenberg, C.; Musil, D.; Bomke, J.; Eggenweiler, H.-M.; Mayer, M. P.; Bukau, B. *PLoS One* **2013**, *8* (11), No. e78443.
(36) Jansen, C.; Sahni, J.; Suzuki, S.; Horgen, F. D.; Penner, R.; Fleig, A. *Sci. Rep.* **2016**, *6* (1), No. 33459.
(37) Visser, D.; Langeslag, M.; Kedziora, K. M.; Klarenbeek, J.; Kamermans, A.; Horgen, F. D.; Fleig, A.; van Leeuwen, F. N.; Jalink, K. *Cell Calcium* **2013**, *54* (6), 404−415.
(38) Kim, B. J.; Nam, J. H.; Kwon, Y. K.; So, I.; Kim, S. J. *Basic Clin. Pharmacol. Toxicol.* **2013**, *112* (2), 83−89.
(39) Ji, D.; Fleig, A.; Horgen, F. D.; Feng, Z.-P.; Sun, H.-S. *Cell Calcium* **2022**, *101*, No. 102521.
(40) Hammad, A. S.; Yu, F.; Al-Hamaq, J.; Horgen, F. D.; Machaca, K. *Cell Calcium* **2023**, *114*, No. 102779.
(41) Sisquella, X.; Nebl, T.; Thompson, J. K.; Whitehead, L.; Malpede, B. M.; Salinas, N. D.; Rogers, K.; Tolia, N. H.; Fleig, A.; O'Neill, J.; Tham, W.-H.; Horgen, F. D.; Cowman, A. F. *eLife* **2017**, *6*, No. e21083.
(42) Zeitlmayr, S.; Zierler, S.; Staab-Weijnitz, C. A.; Dietrich, A.; Geiger, F.; Horgen, F. D.; Gudermann, T.; Breit, A. *Arch. Toxicol.* **2022**, *96* (10), 2767−2783.
(43) Huguet, F.; Calvez, M. L.; Benz, N.; Le Hir, S.; Mignen, O.; Buscaglia, P.; Horgen, F. D.; Férec, C.; Kerbiriou, M.; Trouvé, P. *Cell. Mol. Life Sci. CMLS* **2016**, *73* (17), 3351−3373.
(44) Khalil, A.; Shekh-Ahmad, T.; Kovac, S.; Wykes, R. C.; Horgen, F. D.; Fleig, A.; Walker, M. C. *Epilepsia Open* **2023**, *8*, No. epi4.12773.
(45) Turlova, E.; Ji, D.; Deurloo, M.; Wong, R.; Fleig, A.; Horgen, F. D.; Sun, H.-S.; Feng, Z.-P. *Mol. Neurobiol.* **2023**, *60* (2), 836−850.
(46) Turlova, E.; Bae, C. Y. J.; Deurloo, M.; Chen, W.; Barszczyk, A.; Horgen, F. D.; Fleig, A.; Feng, Z.-P.; Sun, H.-S. *Mol. Neurobiol.* **2016**, *53* (1), 595−610.
(47) Daina, A.; Michielin, O.; Zoete, V. *Sci. Rep.* **2017**, *7* (1), No. 42717.
(48) Meng, S.; Alanazi, R.; Ji, D.; Bandura, J.; Luo, Z.-W.; Fleig, A.; Feng, Z.-P.; Sun, H.-S. *Cell Calcium* **2021**, *96*, No. 102400.
(49) Steinborn, C.; Huber, T.; Lichtenegger, J.; Plangger, I.; Wurst, K.; Magauer, T. *J. Am. Chem. Soc.* **2023**, *145* (21), 11811−11817.
(50) Burns, K.; Englert, G.; Kazlauskas, R.; Murphy, P.; Schonholzer, P.; Wells, R. *Aust. J. Chem.* **1983**, *36* (1), 171.
(51) Iwagawa, T.; Nakamura, K.; Hirose, T.; Okamura, H.; Nakatani, M. *J. Nat. Prod.* **2000**, *63* (4), 468−472.
(52) Kashman, Y.; Saltoun, M.; Rudi, A.; Benayahu, Y. *Tetrahedron Lett.* **1994**, *35* (47), 8855−8858.
(53) Wager, T. T.; Hou, X.; Verhoest, P. R.; Villalobos, A. *ACS Chem. Neurosci.* **2016**, *7* (6), 767−775.
(54) Frisch, M. J.; Trucks, G. W.; Schlegel, H. B.; Scuseria, G. E.; Robb, M. A.; Cheeseman, J. R.; Scalmani, G.; Barone, V.; Petersson, G. A.; Nakatsuji, H.; Li, X.; Caricato, M.; Marenich, A. V.; Bloino, J.; Janesko, B. G.; Gomperts, R.; Mennucci, B.; Hratchian, H. P.; Ortiz, J. V.; Izmaylov, A. F.; Sonnenberg, J. L.; Williams; Ding, F.; Lipparini, F.; Egidi, F.; Goings, J.; Peng, B.; Petrone, A.; Henderson, T.; Ranasinghe, D.; Zakrzewski, V. G.; Gao, J.; Rega, N.; Zheng, G.; Liang, W.; Hada, M.; Ehara, M.; Toyota, K.; Fukuda, R.; Hasegawa, J.; Ishida, M.; Nakajima, T.; Honda, Y.; Kitao, O.; Nakai, H.; Vreven, T.; Throssell, K.; Montgomery, J. A., Jr.; Peralta, J. E.; Ogliaro, F.; Bearpark, M. J.; Heyd, J. J.; Brothers, E. N.; Kudin, K. N.; Staroverov, V. N.; Keith, T. A.; Kobayashi, R.; Normand, J.; Raghavachari, K.; Rendell, A. P.; Burant, J. C.; Iyengar, S. S.; Tomasi, J.; Cossi, M.; Millam, J. M.; Klene, M.; Adamo, C.; Cammi, R.; Ochterski, J. W.; Martin, R. L.; Morokuma, K.; Farkas, O.; Foresman, J. B.; Fox, D. J. *Gaussian 16 Rev. C.01*; Gaussian Inc., 2016.
(55) Larionov, O. V.; Corey, E. J. *J. Am. Chem. Soc.* **2008**, *130* (10), 2954−2955.
(56) Glendening, E. D.; Landis, C. R.; Weinhold, F. *J. Comput. Chem.* **2019**, *40*, No. jcc.25873.
(57) Schmitz, C.; Perraud, A.-L.; Johnson, C. O.; Inabe, K.; Smith, M. K.; Penner, R.; Kurosaki, T.; Fleig, A.; Scharenberg, A. M. *Cell* **2003**, *114* (2), 191−200.

https://doi.org/10.1021/acs.jnatprod.3c00942
J. Nat. Prod. XXXX, XXX, XXX−XXX